UCRL-11391

University of California

Ernest O. Lawrence Radiation Laboratory

INTERACTION OF HIGH ENERGY PROTONS AND HELIUM IONS WITH NIOBIUM

TWO-WEEK LOAN COPY

This is a Library Circulating Copy which may be borrowed for two weeks. For a personal retention copy, call Tech. Info. Division, Ext. 5545

DISCLAIMER

This document was prepared as an account of work sponsored by the United States Government. While this document is believed to contain correct information, neither the United States Government nor any agency thereof, nor the Regents of the University of California, nor any of their employees, makes any warranty, express or implied, or assumes any legal responsibility for the accuracy, completeness, or usefulness of any information, apparatus, product, or process disclosed, or represents that its use would not infringe privately owned rights. Reference herein to any specific commercial product, process, or service by its trade name, trademark, manufacturer, or otherwise, does not necessarily constitute or imply its endorsement, recommendation, or favoring by the United States Government or any agency thereof, or the Regents of the University of California. The views and opinions of authors expressed herein do not necessarily state or reflect those of the United States Government or any agency thereof or the Regents of the University of California.

For
Phys. Rev.

UCRL-11391

UNIVERSITY OF CALIFORNIA

Lawrence Radiation Laboratory
Berkeley, California

AEC Contract No. W-7405-eng-48

INTERACTION OF HIGH ENERGY PROTONS AND HELIUM IONS WITH NIOBIUM

Ralph G. Korteling and Earl K. Hyde

April 1964

INTERACTION OF HIGH ENERGY PROTONS AND HELIUM IONS WITH NIOBIUM*†

Ralph G. Korteling‡ and Earl K. Hyde

Lawrence Radiation Laboratory
University of California
Berkeley, California

April 1964

ABSTRACT

Production cross sections were measured radiochemically for isotopes of niobium, zirconium, copper, nickel, and sodium produced in niobium targets bombarded with 240, 320, 500, and 720 MeV protons and with 320, 500, 720, and 880 MeV helium ions. For the proton bombardments these cross sections were also calculated by the Monte Carlo method with an electronic computer by use of the conventional 2-step model of high energy reactions. Interpolated results of a previous calculation by Metropolis and co-workers were used to simulate the effect of the initial high energy cascade. These results were used in turn as input data for an evaporation calculation. A comparison of the theoretical yields of final products to the observed yields indicates that the theory accounts fairly well for low-deposition energy products (niobium and zirconium isotopes), and quite well for high-deposition energy products (copper and nickel isotopes). The theory fails completely to account for the yields of sodium isotopes, whose production must be ascribed to fragmentation, as noted previously by others.

No Monte Carlo calculations were made for helium-ion induced reactions. However, a comparison of yields of products of helium-ion and proton induced reactions shows a remarkable similarity at all energies and for all products. The main difference is a greater yield by a factor of two in the case of helium-ion bombardments. The implications of this for the mechanism of fragmentation are discussed.

During the course of this work a 15 minute positron emitter was discovered and identified as Nb^{88}.

I. INTRODUCTION

One general method for the investigation of the interaction of high energy particles with complex nuclei is the radiochemical analysis of the heavy radioactive products of such interactions.[1] There exist many published studies of this type for a variety of targets bombarded with protons over the range of a few tens of MeV up to 27 GeV. The results have often been analyzed in terms of proposed mechanisms for the deposition of energy in the nucleus by the incident proton, and for the deexcitation of the excited nucleus by particle evaporation, by fission, or by fragmentation. There have been many fewer experimental studies of the interaction of more complex projectiles such as deuterons or helium nuclei with complex nuclei, chiefly because most high energy accelerators have been designed for the acceleration of protons only. In fact there exist only two accelerators which are equipped to accelerate helium ions in the range of a few hundred MeV up to maximum of about 900 MeV. These are the Berkeley 184 inch synchrocyclotron and the synchrocyclotron of the Joint Institute for Nuclear Research at Dubna in the Soviet Union.

The purpose of the investigation reported here was to carry out a careful study of the reaction products in a typical medium weight target element bombarded alternately with protons and with helium ions under similar experimental conditions and over the energy rangeof 240 to 880 MeV. The comparison of the results was expected to indicate similarities and differences in the interaction of the two types of particles, particularly in the first, or energy deposition, stage of the reaction. It was carried

out as a companion study to one by Crespo, Hyde, and Alexander[2] in which the recoil and yield characteristics of the fragmentation products, Na^{24} and Mg^{28}, were measured in a series of targets bombarded with protons and helium ions over the same energy range.

A second purpose of the investigation was to check with some precision the predictions of a conventional two-step model of high energy nuclear reactions induced by protons. In this model, as discussed in detail in the review article of Hudis and Miller[1], the first step of the reaction is a prompt cascade of nucleon-nucleon collisions. These collisions are initiated by the incoming proton which converts a collection of target nuclei into a collection of struck nuclei with differing numbers of neutrons and protons and differing levels of excitation. The second step is the deexcitation of these excited nuclei by evaporation of neutrons, protons, deuterons and other particles. Monte Carlo methods of calculation of both stages of the reaction have been formulated in past publications by others. However, in only a few instances have these methods been applied in succession to the case of a specific target-projectile combination in order to make detailed predictions of expected reaction products. We have applied the Monte Carlo calculation method in succession to the two-stages of the reactions induced in niobium by protons. Our results are useful both in indicating which parameters are the sensitive ones, particularly in the evaporation deexcitation stage, and in showing to what extent the two-step model is capable of explaining the cross section results.

Niobium was selected as a target material for several reasons. It is monoisotopic and it contains sufficient nucleons for a meaningful calculation of the knock-on and evaporation cascades. Its spectrum of reaction

products is not complicated by the presence of fission products. And, finally, it is available in metallic foils of convenient thickness and sufficient chemical purity.

In an ideal experiment of this nature one would investigate all possible products. Limitations of time and effort led us to investigate only five elements among the numerous products. Isotopes of niobium and zirconium were studied as indicators of reactions in which only a few tens of MeV were deposited in the target. Isotopes of copper and nickel were chosen as indicators of reactions in which some hundreds of MeV of excitation were required. The element sodium was chosen as an indicator of fragmentation products.

We discuss in order the experimental methods, the experimental results, the Monte Carlo calculations, the comparison of experimental and theoretical results, and finally the comparison of the results from the helium-ion and proton induced reactions.

II. EXPERIMENTAL PROCEDURES

A. Target and Monitoring Details

Thin niobium target foils were irradiated in the internal beam of the 184-inch synchrocyclotron of the Lawrence Radiation Laboratory. By use of different radial settings it was possible to select bombardment energies in the range 240-720 MeV for protons and 320-880 MeV for helium ions. We chose the four energies 240, 320, 500, and 720 MeV for the proton experiments and 320, 500, 720, and 880 MeV for the helium-ion experiments. These energies are believed to be correct within an uncertainty of ± 10 MeV. The beam intensity was of the order of 0.5 microampere.

Deuteron contamination of the helium-ion beam was considered to be small. It was certainly negligibly small for the majority of the bombardments, which were conducted days after the last previous use of the cyclotron for deuteron acceleration.

The target arrangement consisted of a stack of foils clamped together in a simple copper target holder which could be readily connected and removed from the internal cyclotron probe. The beam struck the outer edge of the foil stack at right angles to the target. Since the total stack thickness was small compared to the range of the particles, there was multiple traversal of the foils. In order of traversal by the beam, the stack consisted of a 3 mil aluminum guard foil, a 1 mil aluminum monitor foil (of > 99.99% purity), a second 3 mil aluminum guard foil, and a 2.5 mil niobium foil. In the experiments in which sodium production was studied, guard foils of niobium enclosed the target foil to prevent extraneous activity from interfering with the measurement of sodium cross sections. The foils were cut to dimensions 2 × 3.5 cm and milled as a stack on all sides to insure uniform area. Special care was taken to maintain clean surfaces. Since the beam cuts a circular path outward, the alignment of the leading edge of the foil stack was critical. Hence, the machining of the leading edge was made after the stack was mounted in the target holder. Checks were made to establish the correctness of the alignment of the target and monitor foils, and the error due to misalignment was found to be below one percent.

The niobium used in all the irradiations came from the same 2.5 mil sheet, which when analyzed by optical spectroscopy gave the impurity values listed in Table I. The guard foils protected the monitor foil from any background activity resulting from any structural materials of higher Z.

The total proton current passing through the foil stack was determined by measurement of Na^{24} activity produced by the reaction, $Al^{27}(p,3pn)Na^{24}$. The cross section for this reaction is nearly constant over the energy range of interest here and from the careful work of many authors its value is well known.[3] We used a value of 9.5 mb at 240 MeV and of 10.6 mb at our three other bombardment energies.

The integrated helium-ion beam was monitored with the Na^{24} activity produced in the monitor foil by the reaction $Al^{27}(\alpha,\alpha 2pn)Na^{24}$. The excitation function for this reaction has been measured[4,5] only to 380 MeV. At 380 MeV it has the value 24 mb, and it decreases slowly at an unknown rate at higher bombarding energies. We use the value of 24 mb throughout the energy range 320 to 880 MeV. We also quote the ratio of our product cross section to the monitor cross section so that the correction to an absolute cross section value can easily be made later, when better values of the monitor cross section are available.

In some cases when the count-rate of the Na^{24} activity in the monitor foils was too high for accurate determination, the longer-lived Na^{22} was measured instead. The Na^{22} activity was then converted to an equivalent Na^{24} count-rate by a conversion factor determined in a separate set of experiments.

B. Chemical Separations

A short time after each irradiation the niobium foil was dissolved in a mixture of hydrofluoric and nitric acids. Ten to twenty milligrams of zirconium, copper, nickel, and sodium were added to the solution, following which, radiochemical separations were performed to isolate one or more of the product elements of interest in high chemical and radiochemical

purity. Outlines of the methods are given in Appendix A. The final chemical step for each element consisted of the precipitation of a compound of definite composition which was dried and weighed to determine the percentage recovery of the element. Errors in the determination of chemical yield were estimated to be less than 5 percent. The precipitate was filtered onto a glass filter disc to form a sample of approximately 8 mg/cm^2 thickness which was suitably mounted for measurement of its radioactivity.

C. Activity Measurements

The gamma spectrum of each element was measured with a sodium iodide crystal coupled to a multichannel pulse-height analyzer. These spectra served to identify the isotopes present in the sample, to reveal possible impurities, and, in some cases, to calibrate the counting efficiency of the beta counters. All quantitative yield measurements were made by an analysis of decay curves of the activity measured in methane-flow, end-window, proportional counters. These counters were standardized for absolute counting, in cooperation with Blann[6] by the procedure published by Bayhurst and Prestwood.[7] According to this method, an empirical relationship between the efficiency of the counter and the average beta energy is used to determine the counting efficiency for a particular activity. Independent empirical corrections for self absorption, back scattering, etc., were not made. We estimate an absolute error of 5 to 10% on our standardization of counting efficiency. However, since our samples are measured relative to the Na^{24} monitor activity standardized by the same method, the resultant error in the reported cross sections is somewhat less.

Errors in determination of the count-rate were less than two percent and in the resolution of the decay curves into components less than three percent. Errors in the correction for the decay scheme varied for each nuclide. The values which we used[8,9] are listed in Table II.

For any of our reported absolute cross sections we estimate an overall error of 20 percent.

Details of the analysis of activity measurements for individual elements are given in Appendix B.

III. EXPERIMENTAL RESULTS

The experimental cross sections are listed in Tables III and IV in blocks according to bombarding energy. In all cases both the absolute cross section and the ratio of the cross section for the isotope to that for the Na^{24} yield in the aluminum monitor are given. Each block contains the average value of the determined ratios under $\overline{X}$. When more than one measurement was made, a standard error is given under the heading $\sigma_{\overline{X}}$ and the number of determinations under D. The absolute cross section was computed from the average values by use of the Na^{24} monitor cross sections listed in the tables. It is emphasized again that the Na^{24} monitor cross section of 24 mb for helium-ion induced reactions is an estimate and may be progressively incorrect (on the high side) as the helium-ion energy increases.

The results are also displayed graphically in figures 1 through 5.

IV. MONTE CARLO CALCULATIONS OF PRODUCT YIELDS

In this section, we discuss the calculation of reaction product yields on the assumption of the validity of the conventional two-step model.

For the first stage we have used selected results of Metropolis and co-workers[10] to determine the spectrum of struck nuclei and their excitation energies at the end of the prompt cascade. The detailed assumptions and mechanics of the calculation are given in the Metropolis paper so we need only mention some of the main points.

The target nucleus was represented by a degenerate Fermi gas in a square well potential of radius $1.3 \times 10^{-13} A^{1/3}$ cm. The incoming proton was assumed to make a collision with one nucleon in the well. After the collision, if both particles had a final energy greater than the maximum Fermi energy, the collision was allowed; if not, the collision was rejected as unphysical. After the initial collision, both particles were followed separately by Monte Carlo calculations to see whether they made additional collisions before they emerged from the nucleus. When all collision partners had either escaped from the nucleus or been absorbed, a summation was made of the energy of the "holes" in the Fermi gas and the excitation energy of the bound collision partners. The output information consisted of summaries of the following information:

1) The type, number, energy, and angular distribution of emitted particles
2) The type, number, excitation energy, momentum and angular distribution of all residual (struck) nuclei

Metropolis et al.[10] did not use niobium as a target in their calculation but they did consider Ru^{100} which is not much different in composition. We have used their results for Ru^{100} and "transposed" them for the Nb^{93} case by subtracting three units of charge and seven units of mass from each of the residual nuclei at the end of the cascade. This transposition was performed for the three energies of 462, 944, and 1844 MeV, although the third energy falls above the energy range used in our experimental work and will not be discussed in detail.

The transposed output data of the prompt cascade was used as the input information of a Monte Carlo evaporation cascade calculation. We followed closely the calculation outlined by Dostrovsky, Fraenkel, and Friedlander,[11] which in turn is based upon the theoretical ideas of Weisskopf.[12] Dostrovsky et al. used the WEIZAC computer at the Weizmann Institute. We used a program written for the IBM 7090 by Alexander, Altman, and Howry.[13]

Weisskopf[12] expressed the probability per unit time for the emission of particle j with kinetic energy between E and $E+dE$ by the equation

$$P_j(E)dE = \frac{g_j m_j}{\pi^2 \hbar^3} \sigma_c E \, (W_f/W_i) dE. \qquad (1)$$

Here g_j is the number of spin states of j, m_j is the mass of the emitted particle, σ_c is the cross section for the inverse reaction, and W_f and W_i are the level densities of the final and initial states.

For neutron emission, the value of σ_c is obtained from the geometric cross section σ_g via the expression

$$\sigma_c/\sigma_g = \alpha(1 + \beta/E) \tag{2}$$

where α and β are constants obtained from continuum theory.

For charged particle emission, the coulomb barrier must be taken into account. An empirical equation of the form

$$\sigma_c/\sigma_g = (1 + C_j)\,(1 - k_j V_j/E) \tag{3}$$

was used. The factor $(1 - k_j V_j/E)$ is an approximation to the quantum mechanical penetration of the barrier. C_j and k_j are constants which are evaluated from continuum theory. The barrier is computed from the simple classical expression

$$V_j = \frac{zZe^2}{r_0 A^{1/3} + \rho_j} \tag{4}$$

where z and Z are the atomic numbers of the emitted particle and residual nucleus, e is the electronic charge, and ρ_j is an approximation for the radius of the emitted particle. The radius parameter r_0 was set equal to 1.7×10^{-13} cm.

The level density expression of crucial importance to any evaporation calculation based on the Weisskopf theory. Dostrovsky, Fraenkel and Friedlander[11] chose the form

$$W(E) = C \exp\{2[(E-\delta]^{1/2}\} \tag{5}$$

where C is a constant, a is a constant proportional to mass number, E is the energy, and δ is a correction term to adjust for odd-even pairing energy effects. The term δ, in effect, adjusts the position of the ground state energy and was evaluated from Cameron's[14] semi-empirical mass equation. We used the values $A/20$ and $A/10$ for the parameter a.

We must consider also the limits of integration. The maximum energy available for the evaporation process is

$$(\epsilon_n)_{max} = E - Q_n - \delta_n \text{ for neutrons and}$$

$$(\epsilon_j)_{max} = E - Q_j - k_j V_j - \delta_j \text{ for charged particles.}$$

Hence, the integration is carried out over the range of 0 to $E - Q_n - \delta_n$ for neutrons and $k_j V_j$ to $E - Q_j - \delta_j$ for charged particles. Q_n and Q_j are the separation energies.

A combination of the above expressions together with the approximation that

$$\exp\,[2(a_n R_n)^{1/2}] \gg 1 \tag{6}$$

yields the neutron-emission probability

$$\Gamma_n \approx [(m_n r_0^2)/(2\pi\hbar^2)]\,\exp\,\{-2[a_0(E-\delta_0)]^{1/2}\}$$

$$\times\; A_n^{2/3}\;[g_n\alpha/a_n^2]\;\exp\,[2(a_n R_n)^{1/2}] \tag{7}$$

$$\times\; \{2a_n R_n - (3/2 - a_n\beta)\,[2(a_n R_n)^{1/2} - 1]\}$$

where

$$R_n = E - Q_n - \delta_n\,. \tag{8}$$

With the assumption that

$$\exp\,[2(a_j R_j)^{1/2}] \gg 1 \tag{9}$$

one obtains for the probability of charged particle emission

$$\Gamma_j \approx [(m_j r_0^2)/(2\pi\hbar^2)] \exp\{-2[a_0(E-\delta_0)]^{1/2}$$

$$\times A_j^{2/3} [g_j(1+c_j)/a_j^2] \times \exp[2(a_j R_j)^{1/2}] \qquad (10)$$

$$\times \{2a_j R_j - (3/2)[2(a_j R_j)^{1/2} - 1]\}$$

where

$$R_j = E - Q_j - k_j V_j - \delta_j . \qquad (11)$$

These are the basic equations used in the work of Dostrovsky, Fraenkel and Friedlander[11] and of ourselves to calculate the relative probabilities for the emission of neutrons, protons, deuterons, tritons, helium-3 ions, helium-4 ions and other charged aggregates.

The kinetic energy of the emitted particles was selected from a distribution calculated from the original Weisskopf formalism. This is expressed by

$$P(X) = (X/X_{max}) \exp\{a_j X_{max} - [a_j(R_j - X]^{1/2}\} \qquad (12)$$

where $X = E - V$ with $V = k_j V_j$ for charged particles, $V = -\beta$ for neutrons, and X_{max} is given by

$$X_{max} = (1/a_j)[(a_j R_j + 1/4)^{1/2} - 1/2] . \qquad (13)$$

To save computer time the high energy tail was approximated by a Maxwellian distribution.

$$P_m(X) = (X/X_{max}) \exp[1-(X/X_{max})] \qquad (14)$$

All the constants required for solution of the above equations were read into the computer. The atomic number and mass, the excitation energy, and the number of cases to be examined were specified. A random number selected the particles to be emitted from a distribution weighted by the relative emission probability for each particle. The weighting fractions were recomputed at each step of the evaporation chain. Other random numbers selected the kinetic energy of the particle from the calculated kinetic energy distributions. This information determined the result of the first evaporation step and the input data for the next step. The procedure was repeated until the R values (see equation 8 and 11) for all particles were ≤ 0. The computer then was instructed to move on to the next evaporation chain. The information obtained from each evaporation chain was

1) The type, number, and energy of emitted particles
2) The type, number, and residual excitation energy of the final products
3) The detailed evaporation path.

For our purposes, only certain summaries of this information were useful and statistically reliable. The chief summary needed for comparison with experimental data was a table of the final products, giving for each product the Z, A, number of cases, and fraction of the total products.

In most of our calculations we limited the evaporation to the following six particles: neutron, proton, deuteron, triton, helium-3 nucleus, and helium-4 nucleus. In a few test calculations the evaporation of heavier particles numbering 16 in all was permitted. We did not find that this change made an appreciable difference in the yield of the products in which we were interested.

The input information from the Metropolis et al. cascade calculations covered 809 cases at 462 MeV and 695 cases at 944 MeV. The geometric cross section for protons interacting with niobium is ≈ 1200 mb. Hence, the statistical error for any final product with a formation cross section less than a few millibarns was quite large. To reduce somewhat the statistical error in the results five evaporation calculations were performed for each initial cascade case. It also proved helpful to employ certain averaging procedures to smooth out the results. This is possible and proper since the model predicts systematic trends in yield as function of atomic mass and charge. For example, the isobaric distribution could be approximated by a Gaussian curve. The computer results for 3 or more products of different Z at each value of A could be plotted on probability paper to determine a most probable Z, designated Z_p, and the standard deviation σ of the Gaussian distribution. Resulting values for Z_p and σ are shown in figures 6 and 7. In order to obtain a satisfactorily smooth curve of fractional yield versus mass number, it was necessary to average the isobaric yields over 3 mass units. Figure 8 shows one summary of our calculations averaged in this fashion.

With the aid of our curves for Z_p, the charge distribution parameter σ, the isobaric yield curves, and a total cross section value of 1230 mb, obtained by graphical interpolation of the results of Gooding,[15] we were able to calculate the cross section of any isotope. We made such calculations for the isotopes isolated in our work. We discuss these in the next section.

Details of the calculations and the results are given more fully in the thesis study by one of us.[16]

V. COMPARISON OF THE EXPERIMENTAL AND CALCULATED CROSS SECTIONS

Figures 9, 10, 11, and 12 show the calculated yields at two bombbarding energies and the experimental yields at four for the isotopes of niobium, zirconium, copper and nickel studied in our experiments.

A. Low Deposition Energy Processes

The niobium and zirconium results are representative of low deposition-energy processes. The experimental and calculated values are compared in figures 9 and 10. The excitation functions have a negative slope in agreement with the expectation that their maximum cross sections are obtained at much lower bombarding energies than those considered here. This decrease can be attributed to the competition from processes of higher deposition energy as the bombarding energy is increased. The fact that the yields decrease rather slowly is proof that the prompt cascades includes a sizeable proportion of events in which only a small fraction of the energy of the incoming particle is transferred to the target nucleus. The rough agreement of the experimental and theoretical curves shows that the general trend with increasing energy is correctly reproduced.

The calculation underestimates the measured value for Nb^{90} by a factor of 1.7 at 462 MeV and by a larger factor at higher bombarding energies. The agreement for Nb^{89} is satisfactory at 462 MeV but worsens at higher energies. These discrepancies are of the same order as those observed by others for products of the (p,pxn) type when x is a small number.[10,17-20] The comparison of calculated and experimental values for the zirconium isotopes is somewhat better. At 462 MeV the calculation underestimates the values for Zr^{88} and Zr^{89} by about 25%. The experimental

value for Zr^{87} is bracketed by the calculated values based on A/20 and A/10 for the level-density parameter a. There is a gradual worsening of this agreement at higher energies.

B. High Deposition Energy Processes

The experimental cross sections for copper and nickel isotopes show sharply increasing excitation functions. The slopes of these curves are greater for the more neutron-deficient isotopes than for the neutron-excess isotopes. These are the qualitative properties expected from the cascade-evaporation model. The quantitative predictions of the model are presented in figures 11 and 12 and compared with the experimental data.

The agreement in most of these cases can be considered excellent both for the order of magnitude for these small-yield products, and for the slope of the excitation functions. In the cases of Cu^{64}, Cu^{67}, Ni^{66}, and Ni^{65}, the theoretical curves for the two choices of the a-parameter in the level density formula bracket the experimental results. In the case of the very light product Cu^{61} the calculation overestimates the yield, but by less than a factor of 2, which is not serious. The lightest nickel isotope, Ni^{57}, is an exception. It is badly overestimated by the calculation.

We conclude that within the statistical accuracy imposed by the limited number of cascade events considered in the calculation, the yields of the copper and nickel isotopes on the neutron-excess side of beta stability are satisfactorily described by the conventional reaction model. The yields could easily be more closely calculated by an adjustment of the level density parameter within a reasonable range of choices. These cases represent large

deposition energy (300 MeV or more on the average) sufficient for the removal of about 30 units of mass from the target nucleus. The fact that the neutron-deficient isotopes of these elements are not so well calculated may indicate that the charge distribution of yields is improperly estimated.

C. High Deposition Energy Processes Leading to Fragmentation

The production cross sections for Na^{24} and Na^{22} (see figure 5) increase with bombarding energy. Our results follow the systematic trends observed for the production of Na^{24} in other targets by Caretto, Hudis, and Friedlander[21] and by Crespo, Alexander, and Hyde.[2] Our experimental data for Na^{22} are considerably less certain than those for Na^{24}, and in particular, the higher yield of Na^{22} at 240 than at 320 MeV is questionable.

Two features of the excitation functions may be mentioned. First, the slopes are not as great as those for the copper and nickel isotopes; there is only a factor of 10 increase in yield over the range of bombarding energy compared to a factor of about 100 for the copper and nickel isotopes. Second, the ratio of the more neutron-deficient Na^{22} isotope to Na^{24} decreases with increasing bombarding energy, whereas the corresponding ratios for the copper and nickel isotopes increase. Both these observations are contrary to the predictions of the reaction model which would say that the slope of the excitation function and the increasing yield of neutron-deficient over neutron-excess products should be much greater for sodium than for copper and nickel.

Furthermore, the yields of the sodium isotopes are orders of magnitude greater than the cascade-evaporation model would predict. The experimental cross sections are comparable to those for copper and higher than those for nickel, whereas the calculation does not predict the formation of any products with mass < 35 until the bombarding energy is raised above 1 GeV.

We conclude that the sodium isotopes were produced by a reaction mechanism quite distinct from that described by the conventional model which is based on the evaporation of numerous small particles from a highly-excited target nucleus. Our result supports the conclusion reached by many others[1,2,21-24] that an additional mechanism, often called fragmentation, is operative in reactions induced by particles of high energy.

It is interesting to compare our Na^{24} cross sections with those obtained by others from various targets; such a comparison is presented in figure 13. It can be seen that the points for niobium targets correlate with those for other elements. The unusual form of the curves in this figure constitutes part of the evidence for a fragmentation origin for Na^{24} as is discussed by Caretto, Hudis, and Friedlander,[21] and Crespo, Alexander, and Hyde.[2]

VI. DISCUSSION OF RESULTS FOR REACTIONS INDUCED BY HELIUM IONS

The yields of the products for the helium-ion-induced reactions are listed in Tables III and IV and plotted in Figures 1 through 5. The two striking features of the comparison of these yields to those obtained in the proton-induced reactions are the greater yields in the reactions induced by helium ions and the close parallelism of the excitation functions. The yield ratios are summarized in Table V. These ratios are close to the value 2 for all products and all bombarding energies. This is a striking constancy considering the great range of cross section values and the differences in slope for the different products. It seems apparent that the pattern of energy deposition is quantitatively very much the same in the helium-ion bombardments as it is in the proton bombardments.

This is an unexpected result for several reasons. We cite the conclusion for our discussion above and from the previous work of others that the sodium isotopes are formed by a reaction mechanism which is different from that which leads to the production of the heavier products. It seems surprising that the results for both types of reactions should be so similar for the two types of particles. This is particularly so if one accepts the fragmentation mechanism suggested by Wolfgang et al.[22] in which pion formation plays a significant role in transferring large amounts of energy to the struck nucleus. It seems unlikely that an alpha particle would produce pions in nearly the same yield as protons. It is usually stated that a pion can be produced only by the interaction of an individual nucleon with a nucleon in the target nucleus. Each component nucleon of the alpha particle has about one quarter the total energy of the alpha particle, with a

distribution related to the internal momentum. Since the cross section for pion production by a free nucleon is a steep function of energy in the region 100-500 MeV, one would expect fewer pions produced by alpha particles than by protons of the same energy over the range of energies we have studied. The threshold and the steep rise in the meson excitation function should be displaced to higher helium ion energies. This difference in the ability of the two projectiles to produce mesons should be reflected in the production cross sections of products whose formation is influenced in a significant way by meson production and reabsorption. We see no evidence for differences in the production of any of the studied isotopes except that the yields are higher by a factor of 2 in the helium ion experiments.

One might argue that the alpha particle compensates for its lesser pion production and reabsorption by initiating a more complex cascade with its four nucleons. This could well be ture but it seems unlikely to us that this compensatation should be so close for each of the four bombarding energies and for each group of products.

It is not possible to program a Monte Carlo Calculation for the initial fast cascade induced in target nuclei struck by energetic helium nuclei because of insufficient data on elastic and inelastic cross sections of helium ions interacting with nucleons. In particular, the literature does not contain extensive data on the production cross sections for mesons in targets bombarded with helium ions. Another uncertainty is the fate of the helium ion after the first collision. Does it break up and release four fast nucleons in the interior of the target nucleus to propagate separate cascades? Or does it retain its identity throughout the cascade until it is absorbed or escapes from the nucleus? There is some evidence that the latter is the case,

at least for reactions occurring in the surface. Igo, Hansen, and Gooding[25] studied the (α, 2α) reaction in a series of targets bombarded at 910 Mev. They used two particle detectors to measure the identity, energy and angle of the two alpha particles emerging from the target. Their results indicate a strong probability for alpha clusters in the nuclear surface and for a quasi-free elastic collision of the incoming α-particle with an alpha cluster.

The near constant value of 2 (Table V) in the ratios of yields in the helium ion and proton experiments is caused, for the most part, by the larger reaction cross section for the helium ions. Huizenga and Igo[26] give 1628 mb as the reaction cross section for 46 MeV helium ions interacting with a niobium target. For the proton bombardment calculations we have used a value of 1230 mb interpolated from the measurements of Gooding[15] at 34 MeV. These values differ by 32 percent. It could easily be that the total inelastic cross sections for incident particles of 320-720 MeV energy are appreciably different from those determined at 46 and 34 MeV by these authors. It is known, for example, that there exists an approximate 15 percent nuclear transparency effect for a target with a mass in the region of niobium bombarded with protons in the energy range of 150 to 400 MeV. Nuclear Transparency is probably not so pronounced for helium ions. However, no experimental measurements exist for the total reaction cross section for targets near niobium bombarded with protons and helium ions at these energies.

It is appropriate here to call attention to two other recent studies of spallation reactions with high energy helium ions and protons. L. Miller[27] has compared the (p,pn) and ($\alpha\alpha$n) reactions on Co^{59} targets with protons and helium ions in the same energy range used by us. He finds a marked similarity in the results. L. Winsberg[28] has studied the properties of the alpha-emitter Tb^{149} produced in the bombardment of tantalum and gold

targets with protons ranging from 0.45 to 6.2 GeV and with helium ions of 0.5, 0.7 and 0.88 GeV. This product is about 30 mass units removed from the tantalum target and hence can be compared, at least roughly, with our copper and nickel products for niobium targets. Winsberg measured production cross sections and recoil properties and made a detailed analysis on the basis of the conventional 2-step model. He concluded that the model can account satisfactorily for the results. There is a marked similarity in the cross section values and in the overall recoil properties for the reactions induced by helium ions and protons of the same energy. There are however some indications of significant differences in the initial stage of the reaction induced by the two projectiles.

CONCLUSION

The comparison of our experimental results for proton-induced reactions with detailed calculations based on the conventional 2-stage model of high energy reactions, shows that a wide variety of products produced by low and high energy transfers are moderately well described by the model. However, there is one group of products (the sodium isotopes) which require a separate mechanism (fragmentation).

The results for the helium ion reaction are remarkably similar to the proton results for all groups of products indicating that the energy deposition process is nearly the same. Together with the study of Na^{24} fragmentation products reported by Crespo, Alexander, and Hyde,[2] our results indicate that fragmentation induced by helium ions is closely similar to that induced by protons. This result raises some unresolved questions about the high energy cascade in reactions leading to fragmentation.

ACKNOWLEDGMENTS

We wish to acknowledge the interest and support of Professor I. Perlman in this work. Dr. John M. Alexander contributed many helpful suggestions on the evaporation program and provided us with much of the detailed input information. We are also grateful to him for discussions of the results. Mr. Lawrence L. Altman gave us invaluable help in the adaptation of the evaporation program to the needs of our study. We are grateful to Mr. Herbert C. Albrecht for the conversion of the initial cascade data to a form acceptable by the evaporation program. The assistance of the 184-inch cyclotron operating crew and of the Health Chemistry Group in conducting the bombardments is appreciated. We thank the analytical chemistry group for help in the analysis of our final samples.

APPENDIX A. CHEMICAL PROCEDURES[29]

Preliminary Steps. The foils were snipped from the target after the irradiations to produce a uniform set of foils. After the niobium and aluminum pieces were weighed, the niobium foil was placed in a cellulose-nitrate tube and the aluminum foil was stored for later mounting and counting. A cellulose nitrate tube was used for the dissolution of the niobium rather than glass because a corrosive mixture of concentrated hydrofluoric and nitric acids was employed to dissolve the niobium. After complete dissolution, the excess fluoride ion was removed by successive precipitation of calcium fluoride and barium fluorozirconate. These precipitates were removed by centrifugation and the supernatant solution was transferred to glass equipment.

To this point the chemical treatment was the same for each case.

Niobium Separation Procedure. Niobium pentoxide was precipitated from the above target solution by digestion with potassium bromate in a water bath. The oxide was washed with a solution of dilute nitric acid and ammonium hydroxide, transferred to a cellulose-nitrate tube, and dissolved in concentrated hydrofluoric acid. After a barium flourozirconate precipitation, niobium pentoxide was precipitated with concentrated ammonium hydroxide, washed with a dilute solution of ammonium and sodium hydroxide, and dissolved by digestion with nitric and oxalic acids. A second acid precipitation of niobium pentoxide was carried out on an aliquot of the solution by adding potassium bromate and heating the solution. The niobium pentoxide was filtered through a weighed paper filter and washed with water, alcohol, and acetone. The sample was weighed and mounted in this form. After counting the sample, the precipitate was ignited and weighed to determine the chemical yield. The procedure took approximately 40 minutes.

Zirconium Separation Procedure. Twenty milligrams of zirconium carrier were added to the initial target solution. Addition of barium ion caused the precipitation of barium fluorozirconate which was washed with water and dissolved in concentrated nitric acid containing 5% boric acid. The barium ion was eliminated by the addition of sulfuric acid. Zirconium hydroxide was formed by addition of ammonium hydroxide, and, after a water wash, it was dissolved in concentrated hydrochloric acid. The solution was adjusted to 6 N hydrochloric acid and contacted with a 0.4 M solution of thenoyltrifluoroacetone (TTA) in benzene. The organic phase (containing the zirconium) was washed three times with 1 M nitric acid and contacted with 4 N hydrofluoric acid to back extract the zirconium. The first part of the procedure was repeated up to the TTA extraction step. An aliquot of the solution was then precipitated by digestion with 16% mandelic acid. The zirconium tetramandelate was washed with hot water and filtered through a tared glass filter and again washed with water, alcohol, and ether. After drying for 10 min. at 110°C, the sample was weighed and mounted. The chemical separation took about 1.5 hours.

Copper Separation Procedure. Fifty milligrams of copper carrier and milligram quantities of salts of a number of elements near copper and niobium in atomic number were added to the dissolved target. Excess fluoride ion was removed by the standard method. Upon addition of an excess of ammonium hydroxide, the copper remained in solution as the ammonium complex while the niobium, and many other elements, precipitated as the hydroxide. The solution was adjusted to 2N hydrochloric acid and cupric sulfide was precipitated. Concentrated hydrochloric and nitric acids dissolved the sulfide, and the addition of sodium sulfite reduced the copper to the plus-one state. Addition of potassium

thiocyanate precipitated cuprous thiocyanate which was dissolved with concentrated hydrochloric and nitric acids. Niobium, zirconium, yttrium, and iron ions were added and precipitated as mixed hydroxides to remove contaminants. The copper was then reduced to the metallic form by sodium hydrosulfite in a strongly basic solution. The metallic copper was dissolved in nitric acid, and the procedure was repeated starting at the thiocyanate precipitation. The copper was filtered through a weighed glass filter, washed with water and acetone, weighed, and mounted. Approximately 45 minutes were required for the separation.

Nickel Separation Procedure. Ten milligrams of nickel carrier together with milligram quantities of a number of elements in the region of niobium were added to the target solution. Following the elimination of the fluoride ion, an excess of ammonium hydroxide was added to precipitate the niobium and a number of the other hydroxides, leaving nickel in solution in the form of the ammonium complex. A copper-sulfide precipitation was followed by a precipitation of the mixed hydroxides of zirconium, yttrium, and iron. The nickel was then precipitated with 1 per cent dimethylglyoxime and redissolved in hydrochloric acid. A second copper sulfide precipitation succeeded by a dimethylglyoxime precipitation yielded a sample free from contamination. The precipitate was filtered through a tared glass filter and washed with water. After drying for 10 minutes at 110°C, the sample was weighed and mounted. The procedure took about one hour.

Sodium Separation Procedure. Twenty milligrams of sodium carrier were added to the dissolved target, and the fluoride ion was eliminated. Addition of ammonium hydroxide precipitated the niobium. Copper was added to the supernate to precipitate cupric sulfide as a scavenge. Iron hydroxide was then precipitated for the same purpose. The solution was evaporated

to dryness and 6 M ammonium acetate was added. Sodium was precipitated by stirring with a solution of uranyl acetate, magnesium acetate, and acetic acid, and washed with a solution of glacial acetic acid, anhydrous ethyl acetate, and anhydrous ethanol. The sodium uranyl acetate was suspended in n-butanol. N-butanol saturated with dry hydrogen chloride was added to change the precipitate to sodium chloride which was washed with a solution of n-butanol and n-butanol saturated with hydrogen chloride. The sodium precipitation was repeated, and the organic material was expelled by heating. A small amount of potassium ion was added together with perchloric acid, and the solution fumed to dryness. N-butanol was added and the mixture was boiled to dissolve the sodium perchlorate. Sodium chloride was again precipitated from the supernate by addition of n-butanol saturated with hydrogen chloride. The precipitate was filtered through a tared glass filter, washed with n-butanol, dried for 10 minutes at 110°C, weighed, and mounted. The separation took approximately 3.5 hours.

APPENDIX B. DETAILS OF ACTIVITY MEASUREMENTS

Niobium. The amounts of Nb^{89} and Nb^{90} in the purified niobium fraction were measured by the resolution of the decay curves taken in the proportional counter. Activity contributions from Nb^{91m}, Nb^{92}, and Nb^{95} were also observed but no quantitative measurement of them was attempted. For Nb^{89} the experimentally observed half life of 1.79 hours was used in the analysis of the decay curve. The contribution to the Nb^{89} yield from decay of isobars of higer atomic number was estimated to be less than 10 percent. The growth of 79 hour Zr^{89} into the sample interfered with the measurement of Nb^{90}; this interference was eliminated by repeating the niobium chemical separation 24 hours after bombardment on an aliquot of the niobium fraction, after which the Nb^{90} could be observed free of Zr^{89} contamination. The measured Nb^{90} yield was judged to be the independent yield of this nuclide because of the expected low yield of Mo^{90} and because the 5.7 hour Mo^{90} half life is long compared to the time of the initial Nb separation.

Discovery of Niobium 88. During the course of these experiments a 15 minute positron activity was observed in the niobium fraction and it was established that this activity was the parent of Zr^{88}. This conclusion was confirmed by preparation of the Nb^{88} activity by the reaction of carbon nuclei with a bromine target in the Berkeley Heavy Ion Linear Accelerator. Details of this identification will be published elsewhere.

Zirconium. Zr^{87}, Zr^{88}, and Zr^{89} were measured by analysis of the decay curves of the zirconium fractions taken on the proportional counter. Zr^{86} activity was also observed but certain difficulties in the measurement of this electron-capture activity prevented an absolute determination of yield.

The proportional counter activity of the 85 day Zr^{88} was due to the conversion electrons of the 394 keV gamma transition present in 100 percent abundance. Quantitative measurements of the 394 keV photopeak in the NaI crystal counter made it possible to calibrate the beta counter for Zr^{88} counting. Measurement of the 79 hour Zr^{89} was hampered by the growth of 80 hour Y^{87} from the decay of its 1.6 hour parent, Zr^{87}. This interference was eliminated by a second purification of an aliquot of zirconium 24 hours after bombardment, when the Zr^{87} had decreased below detectability.

The complex decay curves were analyzed with a least squares program on an IBM 704 computer. Good fits were obtained for the three measured isotopes with half life values in agreement with published values.

The yield values for Zr^{87} and Zr^{88} include contributions from isobars of higher Z which were judged to be less than 20 percent of the total. The yield value of Zr^{89} contains only a slight contribution from Nb^{89} because less than 10% of the 1.79 hour Nb^{89} could have decayed into Zr^{89} before the initial chemical separation was made.

In a few cases the results from the analysis of the proportional counter decay curves were checked by measurement of gamma ray photopeaks in the NaI crystal spectrometer and by application of known information on gamma ray energies and intensities.

Copper. Ten minute Cu^{62} and 5 minute Cu^{66} were observed in copper fractions isolated by a rapid chemical procedure, but owing to experimental difficulties we did not complete an accurate determination of their yield. There was little difficulty in resolving 3.3 hour Cu^{61}, 12.0 hour Cu^{64}, and 62 hour Cu^{67} components from the decay curve taken with the aid of the proportional counter on the copper fraction purified by the longer procedure described

in Appendix A. The contributions of isobars of higher atomic number to the Cu^{67} yield is believed to be < 1 percent, and to the Cu^{61} yield, less than 10 percent.

Nickel. Ni^{57}, Ni^{65}, and Ni^{66} components were resolved from the decay curves taken in the proportional counter. Application of the Biller-plot method[30] helped in the separation of the 36 hour Ni^{57} and 54.8 hour Ni^{66}. The contribution of Cu^{57} to the Ni^{57} yield and of Co^{65} and Co^{66} to the yield of Ni^{65} and Ni^{66} is believed to be small as judged from the general observation of a rapid drop off in yield with distance from the line of beta stability.

Sodium. A 15 hour Na^{24} component and a constant Na^{22} component were resolved from the curves taken with the proportional counter. Calibration errors are small since the same nuclides were counted in the monitor foils. However, the counting rates for the 2.6 year Na^{22} were only 1 to 30 counts per minute so that at times there was a considerable error in the subtraction of the background. The measured cross section values include contributions from isobars with $Z \neq 11$. Whether this contribution is large or small is difficult to estimate since there is no systematic information on isobaric yields, and furthermore the mode of production of these light products is unknown.

REFERENCES AND FOOTNOTES

*This work was done under the auspices of the U. S. Atomic Energy Commission.

†Based on a thesis submitted by Ralph G. Korteling to Department of Chemistry, University of California, Berkeley, California.

‡Present address, Department of Chemistry, Carnegie Institute of Technology, Pittsburgh.

1. See review article by J. M. Miller and J. Hudis, Ann. Rev. Nucl. Sci. 9, 159 (1959).
2. V. P. Crespo, J. M. Alexander, and E. K. Hyde, Phys. Rev. 131, 1763 (1963).
3. See review article by J. B. Cumming, Ann. Rev. Nucl. Sci. 13, 261 (1963).
4. M. Lindner and R. N. Osborne, Phys. Rev. 91, 342 (1953).
5. W. E. Crandall, G. P. Millburn, R. V. Pyle, and W. Birnbaum, Phys. Rev. 101, 329 (1956).
6. H. M. Blann, University of California, Lawrence Radiation Laboratory report, UCRL-9190, May 1960, unpublished.
7. B. P. Bayhurst and R. J. Prestwood, Nucleonics 17, No. 3, 82 (1959).
8. Nuclear Data Sheets, National Academy of Sciences, National Research Council (U. S. Government Printing Office, Washington 25, D. C., (1960).
9. D. Strominger, J. M. Hollander, and G. T. Seaborg, "Table of Isotopes" Rev. Mod. Phys. 30, 583 (1958).
10. N. Metropolis, R. Bivens, M. Strom, A. Turkevich, J. M. Miller, and G. Friedlander, Phys. Rev. 110, 185 (1958); ibid. 110, 204 (1958).

11. I. Dostrovsky, Z. Fraenkel, and G. Friedlander, Phys. Rev. 116, 683 (1959).

12. V. Weisskopf, Phys. Rev. 52, 295 (1937).

13. J. M. Alexander, L. Altman, and S. Howry, Lawrence Radiation Laboratory, unpublished work, 1962.

14. A. G. W. Cameron, Atomic Energy of Canada Ltd. report CRP-690, 1957 and Can. J. Phys. 35, 1021 (1958).

15. T. J. Gooding, Nucl. Phys. 12, 241 (1959).

16. R. G. Korteling, University of California, Lawrence Radiation Laboratory, report UCRL-10461 (1962).

17. I. M. Ladenbauer and L. Winsberg, Phys. Rev. 119, 1368 (1960).

18. S. S. Markowitz, F. S. Rowland, and G. Friedlander, Phys. Rev. 112, 1295 (1958).

19. A. A. Caretto and G. Friedlander Phys. Rev. 110, 1169 (1958).

20. N. T. Porile, Phys. Rev. 125, 1379 (1962).

21. A. A. Caretto, J. Hudis, and G. Friedlander, Phys. Rev. 110, 1130 (1958).

22. R. Wolfgang, E. W. Baker, A. A. Caretto, J. B. Cumming, G. Friedlander, and J. Hudis, Phys. Rev. 103, 394 (1956).

23. J. B. Cumming, S. Katcoff, N. T. Porile, S. Tanaka, and A. Wyttenbach, submitted to Phys. Rev. (1964).

24. N. A. Perfilov, O. V. Lozhkin, and V. P. Shamov, Usp. Fiz. Nauk 60, 3 (1960); Uspekhi 3, 1 (1960).

25. G. Igo, L. F. Hansen, and T. J. Gooding, Phys. Rev. 131, 337 (1963).

26. J. R. Huizenga and G. Igo, Nucl. Phys. 29, 462 (1962).

27. L. Miller, thesis, Department of Chemistry, University of California, Davis, California (1964).

28. L. Winsberg, "Recoil Studies of Nuclear Reactions Induced by High-Energy Particles. I. The Production of Tb^{149}", submitted to the Physical Review (1964).

29. Our procedures are based on those published in the following reports: Collected Radiochemical Procedures, Los Alamos Scientific Laboratory Report, LA-1721, Los Alamos, New Mexico, December 1954 and W. W. Meinke, University of California Radiation Laboratory Report UCRL-432 August (1949).

30. W. F. Biller, University of California, Lawrence Radiation Laboratory, Report UCRL-2067, December 1952, unpublished.

Table I. Impurities in the niobium foil.

Impurity	Percent	Impurity	Percent
Oxygen	0.03	Titanium	0.01
Nitrogen	0.03	Tungsten	less than 0.01
Carbon	0.015	Zirconium	less than 0.005
Tantalum	0.05	Nickel	less than 0.005
Iron	0.015		

Table II. Decay properties of investigated nuclides.

Nuclide	Half-life	Rad.	Energy (MeV)	%
Nb-90	14.7 h	β^+	1.50	50
		e^-	0.114	11
		e^-	0.123	19
Nb-89	1.79h	β^+	2.86	91
Zr-89	79.3 h	β^+	0.90	30
		γ	0.915	100
Sr-87m	2.75h	e^-	0.363	22
Zr-88	85d	γ	0.394	100
		e^-	0.377	4.62
Y-88	105d	β^+	0.57	0.7
Zr-87	1.57h	β^+	2.10	83
Zr-86	17h	γ	0.241	100
Y-86	14.6 h	β^+	0.90	3
		β^+	1.32	15
		β^+	1.41	5
		β^+	2.09	6
Y-87m	14h	e^-	0.363	22
Cu-67	61.6 h	β^-	0.395	45
		β^-	0.484	35
		β^-	0.577	20
		e^-	0.083	≈20
Cu-64	12.88h	β^-	0.573	38
		β^+	0.656	19
Cu-61	3.32h	β^+	0.56	3
		β^+	0.94	5
		β^+	1.15	1.1
		β^+	1.21	53.1
Ni-66	54.8 h	β^-	0.20	100
Cu-66	5.10m	β^-	1.59	9
		β^-	2.63	91
Ni-65	2.56h	β^-	0.60	23
		β^-	1.01	8
		β^-	2.10	69
Ni-57	36h	β^+	0.849	39.9
		β^+	0.712	5.6
Na-24	15h	β^-	1.391	100
Na-22	2.58y	β^+	0.554	89.8

Table III. Product cross sections from proton bombardments of niobium

240-MeV Protons on Niobium					320-MeV Protons on Niobium			
Cross section* (mb)	$\bar{X}$	$\sigma_{\bar{X}}$	D	Product	Cross section* (mb)	$\bar{X}$	$\sigma_{\bar{X}}$	D
65.6	6.90		1	Nb-90	54.8	5.17	0.50	2
25.0	2.63		1	Nb-89	21.7	2.05		1
62.7	6.60	2.5×10^{-2}	2	Zr-89	59.7	5.63		1
80.9	8.52		1	Zr-88	71.7	6.76		1
46.7	4.92		1	Zr-87	42.4	4.00		1
1.46×10^{-3}	1.54×10^{-4}	4.5×10^{-6}	2	Cu-67	5.20×10^{-3}	4.91×10^{-4}	2.5×10^{-5}	2
2.09×10^{-2}	2.20×10^{-3}	1.5×10^{-4}	2	Cu-64	0.103	9.75×10^{-3}	2.6×10^{-4}	2
5.18×10^{-3}	5.45×10^{-4}	6.2×10^{-5}	2	Cu-61	3.42×10^{-2}	3.23×10^{-3}	1.4×10^{-4}	2
1.03×10^{-4}	1.08×10^{-5}		1	Ni-66	3.80×10^{-4}	3.58×10^{-5}		1
5.50×10^{-4}	5.79×10^{-5}		1	Ni-65	3.15×10^{-3}	2.97×10^{-4}		1
3.49×10^{-4}	3.67×10^{-5}		1	Ni-57	1.77×10^{-3}	1.67×10^{-4}		1
8.21×10^{-3}	8.64×10^{-4}		1	Na-24	1.48×10^{-2}	1.40×10^{-3}	4.0×10^{-5}	2
1.92×10^{-2}	2.04×10^{-3}	1.3×10^{-4}	2	Na-22	1.59×10^{-2}	1.50×10^{-3}	1.9×10^{-4}	2

Table III. Continued

500-MeV Protons on Niobium				720-MeV Protons on Niobium				
Cross section* (mb)	$\bar{X}$	$\sigma_{\bar{x}}$	D	Product	Cross section* (mb)	$\bar{X}$	$\sigma_{\bar{x}}$	D
47.4	4.47	0.24	2	Nb-90	37.0	3.49	0.35	2
17.7	1.67		1	Nb-89	13.9	1.31		1
44.8	4.23	2.5×10^{-2}	2	Zr-89	38.5	3.63		1
54.2	5.11		1	Zr-88	42.1	3.97		1
32.8	3.09		1	Zr-87	26.1	2.46		1
2.94×10^{-2}	2.77×10^{-3}	1.6×10^{-5}	2	Cu-67	0.119	1.12×10^{-2}	4.7×10^{-4}	3
0.731	6.90×10^{-2}	3.4×10^{-3}	2	Cu-64	2.79	0.263	1.3×10^{-2}	3
0.416	3.92×10^{-2}	3.5×10^{-3}	2	Cu-61	1.73	0.163	1.0×10^{-2}	3
2.86×10^{-3}	2.70×10^{-4}	3.5×10^{-6}	2	Ni-66	8.30×10^{-3}	7.83×10^{-4}	1.5×10^{-5}	2
2.20×10^{-2}	2.08×10^{-3}	1.3×10^{-4}	2	Ni-65	6.28×10^{-2}	5.92×10^{-3}	1.0×10^{-5}	2
1.83×10^{-2}	1.73×10^{-3}	1.5×10^{-4}	2	Ni-57	7.30×10^{-2}	6.89×10^{-3}	3.5×10^{-5}	2
4.27×10^{-2}	4.03×10^{-3}	1.2×10^{-4}	2	Na-24	0.130	1.23×10^{-2}	1.0×10^{-4}	2
2.57×10^{-2}	2.42×10^{-3}	1.0×10^{-4}	2	Na-22	7.29×10^{-2}	6.88×10^{-3}	9.0×10^{-5}	2

*Na^{24} monitor cross section taken as 9.5 mb for 240 MeV p, and as 10.6 mb for 320, 500, and 720 MeV protons.

$\bar{X}$ = ratio of product cross section to Na^{24} monitor cross section.

$\sigma_{\bar{x}}$ = standard error of X when number of determinations D is greater than 1.

Table IV. Product cross sections from helium-ion bombardments of niobium targets.

320-MeV Helium ions on Niobium				500-MeV Helium ions on Niobium				
Cross section* (mb)	$\bar{X}$	$\sigma_{\bar{X}}$	D	Product	Cross section* (mb)	$\bar{X}$	$\sigma_{\bar{X}}$	D
129	5.37	0.27	2	Nb-90	97.2	4.05	0.31	2
46.8	1.95		1	Nb-89	35.5	1.48		1
111	4.61		1	Zr-89	81.4	3.39	3.0×10^{-2}	
145	6.04		1	Zr-88	105	4.38		1
92.2	3.84		1	Zr-87	65.8	2.74		1
1.08×10^{-2}	4.49×10^{-4}	1.0×10^{-5}	3	Cu-67	7.15×10^{-2}	2.98×10^{-3}	1.6×10^{-4}	3
0.173	7.19×10^{-3}	8.3×10^{-4}	3	Cu-64	0.145	6.05×10^{-2}	1.7×10^{-3}	3
$4.42\ 10^{-2}$	1.84×10^{-3}	7.0×10^{-5}	3	Cu-61	6.50×10^{-1}	2.71×10^{-2}	1.0×10^{-3}	3
1.06×10^{-3}	4.40×10^{-5}		1	Ni-66	7.30×10^{-3}	3.04×10^{-4}		1
6.07×10^{-3}	2.53×10^{-4}		1	Ni-65	4.08×10^{-2}	1.70×10^{-3}		1
5.40×10^{-3}	2.25×10^{-4}		1	Ni-57	3.60×10^{-2}	1.50×10^{-3}		1
4.32×10^{-2}	1.80×10^{-3}		1	Na-24	0.113	4.70×10^{-3}		1
4.68×10^{-2}	1.95×10^{-3}		1	Na-22	8.64×10^{-2}	3.60×10^{-3}		1

Table IV. Continued

720-MeV Helium ions on Niobium				880-MeV Helium ions on Niobium				
Cross section* (mb)	$\bar{X}$	$\sigma_{\bar{X}}$	D	Product	Cross section* (mb)	$\bar{X}$	$\sigma_{\bar{X}}$	D
83.5	3.48	0.10	2	Nb-90	72.2	3.01	0.15	3
27.8	1.16		1	Nb-89	27.1	1.13	$6.0\ 10^{-2}$	2
73.9	3.08		1	Zr-89	63.1	2.63		1
93.1	3.88		1	Zr-88	79.7	3.32		1
55.9	2.33		1	Zr-87	47.8	1.99		1
0.166	6.91×10^{-3}	2.6×10^{-4}	2	Cu-67	0.257	1.07×10^{-2}	9.8×10^{-4}	4
4.34	0.181	3.5×10^{-3}	2	Cu-64	6.26	0.261	9.6×10^{-3}	4
2.59	0.108	2.0×10^{-3}	2	Cu-61	4.75	0.198	1.4×10^{-2}	4
1.92×10^{-2}	8.02×10^{-4}		1	Ni-66	2.86×10^{-2}	1.19×10^{-3}	6.1×10^{-5}	3
0.121	5.06×10^{-3}		1	Ni-65	0.167	6.97×10^{-3}	4.2×10^{-4}	3
0.143	5.96×10^{-3}		1	Ni-57	0.242	1.01×10^{-2}	8.3×10^{-4}	3
0.300	1.25×10^{-2}		1	Na-24	0.533	2.22×10^{-2}		1
0.196	8.18×10^{-3}		1	Na-22	0.254	1.06×10^{-2}	1	1

*Na^{24} monitor cross section taken as 24 mb for all energies.
For meaning of $\bar{x}$ and $\sigma_{\bar{x}}$ see footnotes of Table III.

Table V.

Ratio of the cross sections from helium-ion bombardments to those from proton bombardments.

Nuclide	320 MeV	500 MeV	720 MeV	Average
Nb-90	2.33	2.03	2.24	2.20
Nb-89	2.13	1.99	1.99	2.04
Zr-89	1.84	1.80	1.90	1.85
Zr-88	2.01	1.92	2.19	2.04
Zr-87	2.15	1.99	2.12	2.09
Cu-67	2.05	2.42	1.38	1.95
Cu-64	1.65	1.97	1.54	1.72
Cu-61	1.28	1.55	1.49	1.44
Ni-66	2.76	2.53	2.29	2.53
Ni-65	1.91	1.83	1.92	1.89
Ni-57	3.03	1.94	1.94	2.29
Na-24	2.89	2.62	2.29	2.60
Na-22	2.92	3.34	2.27	2.84
Average	2.23	2.15	1.97	

FIGURE CAPTIONS

Figure 1. Production cross section of niobium isotopes in niobium targets bombarded with high energy protons (shown by circles) and high energy helium ions (shown by squares).

Figure 2. Production cross sections of zirconium isotopes in niobium targets bombarded with high energy protons (shown by circles) and high energy helium ions (shown by squares).

Figure 3. Production cross sections of copper isotopes in niobium targets bombarded with high energy protons (shown by circles) and high energy helium ions (shown by squares).

Figure 4. Production cross sections of nickel isotopes in niobium targets bombarded with high energy protons (shown by circles) and high energy helium ions (shown by squares).

Figure 5. Production cross sections of sodium isotopes in niobium targets bombarded with high energy protons (shown by circles) and high energy helium ions (shown by squares).

Figure 6. Variation in calculated value of most probable nuclear charge Z_p with mass number of reaction product. Niobium target bombarded with protons. Data is for $a = A/20$ and the emission of 6 types of particles.

Figure 7. Width of the distribution in charge of the final products as a function of mass number. Calculated value of averaged Gaussian half-widths at half maximum, $(2 \ln 2)^{1/2}\sigma$, for niobium targets bombarded with protons. Results shown for 2 values of the evaporation parameter: $a = A/20$ and $a = A/10$.

Figure 8. Averaged mass-yield curve from the Monte Carlo cascade-evaporation calculation for reaction of protons with niobium. Data are for $a = A/20$ and the emission of six types of particles.

Figure 9. Experimental production cross sections for niobium isotopes (solid symbols) compared to calculated values (open symbols). Broken curve indicates trend of calculated results for evaporation parameter $a = A/10$; dot-dash curve shows trend for $a = A/20$.

Figure 10. Experimental production cross sections for zirconium isotopes (solid symbols) compared to calculated values (open symbols). Broken curve indicates trend of calculated results for evaporation parameter $a = A/10$; dot-dash curve shows trend for $a = A/20$.

Figure 11. Experimental production cross sections for copper isotopes (solid symbols) compared to calculated values (open symbols). Broken curve indicates trend of calculated results for evaporation parameter $a = A/10$; dot-dash curve shows trend for $a = A/20$.

Figure 12. Experimental production cross sections for nickel isotopes (solid symbols) compared to calculated values (open symbols). Broken curve indicates trend of calculated results for evaporation parameter $a = A/10$; dot-dash curve shows trend for $a = A/20$.

Figure 13. Formation cross section for Na^{24} as a function of mass of target for proton and helium ion induced reactions. Niobium points are from this work. The data at 1 and 2 GeV are from Caretto, Hudis, and Friedlander (see footnote 21). The rest are

Figure 13. (Cont.) from Crespo, Alexander, and Hyde (see footnote 2). Proton data are given by circles, helium-ion data by squares. The niobium points are solid.

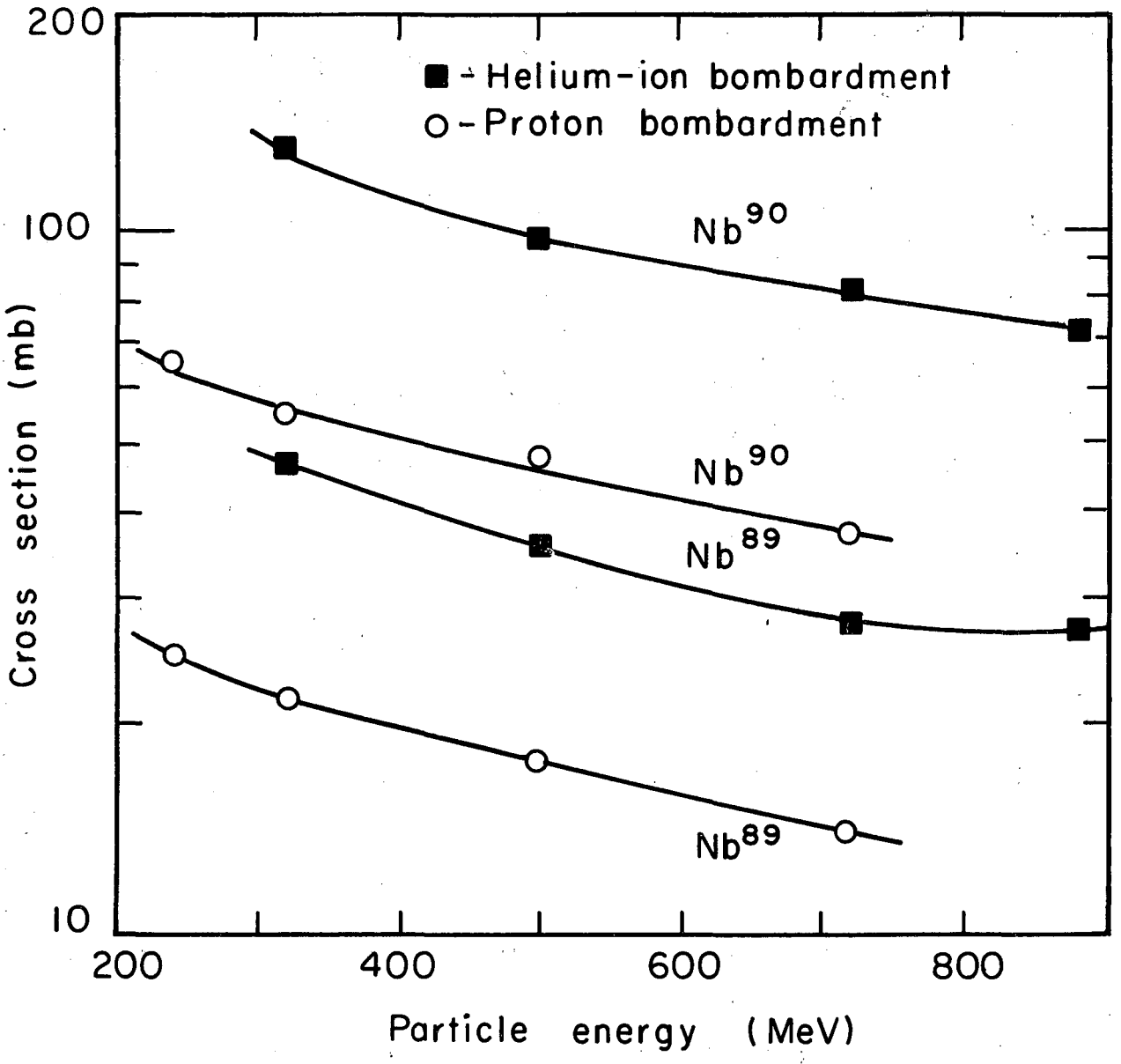

MUB-2764

Fig. 1

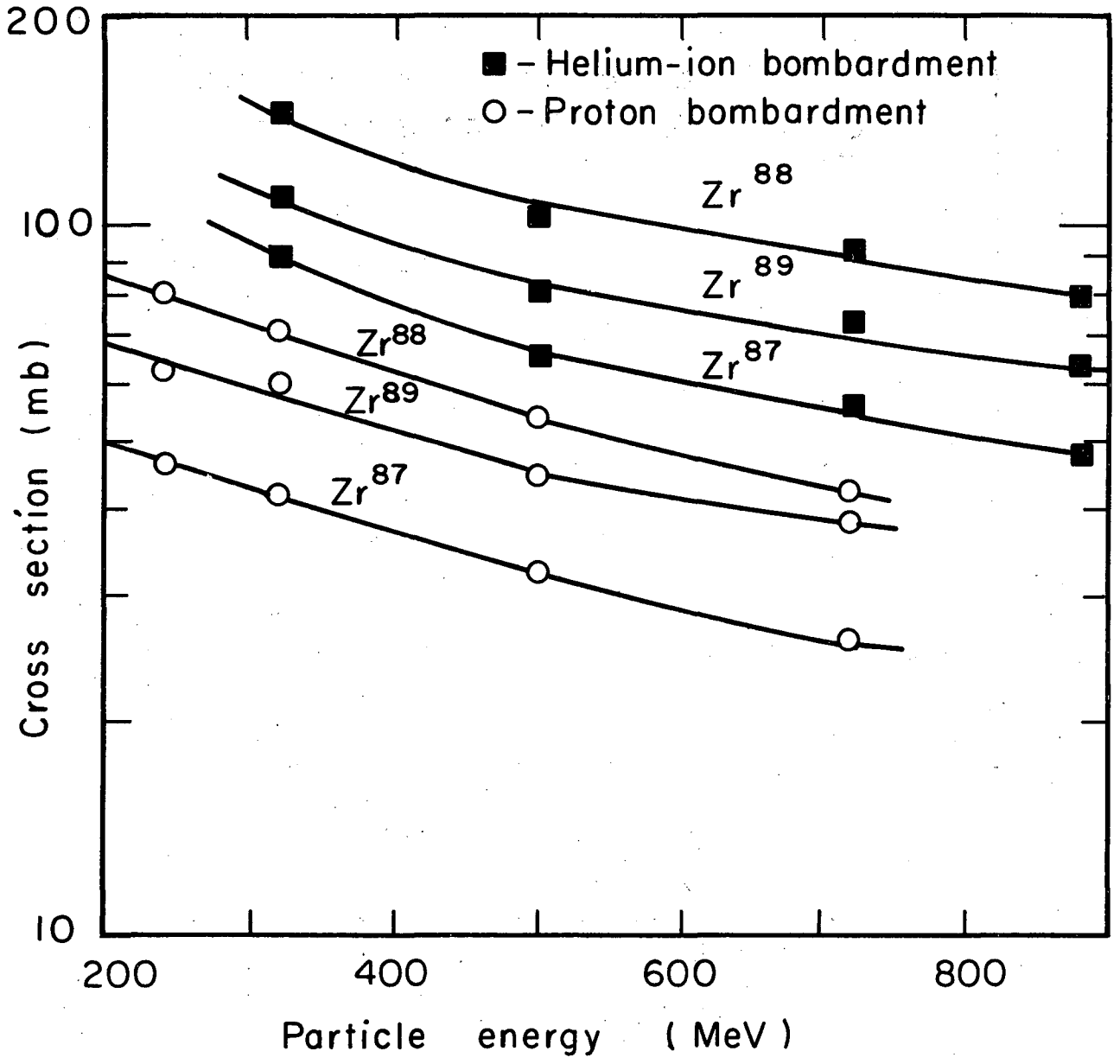

MUB-2765

Fig. 2

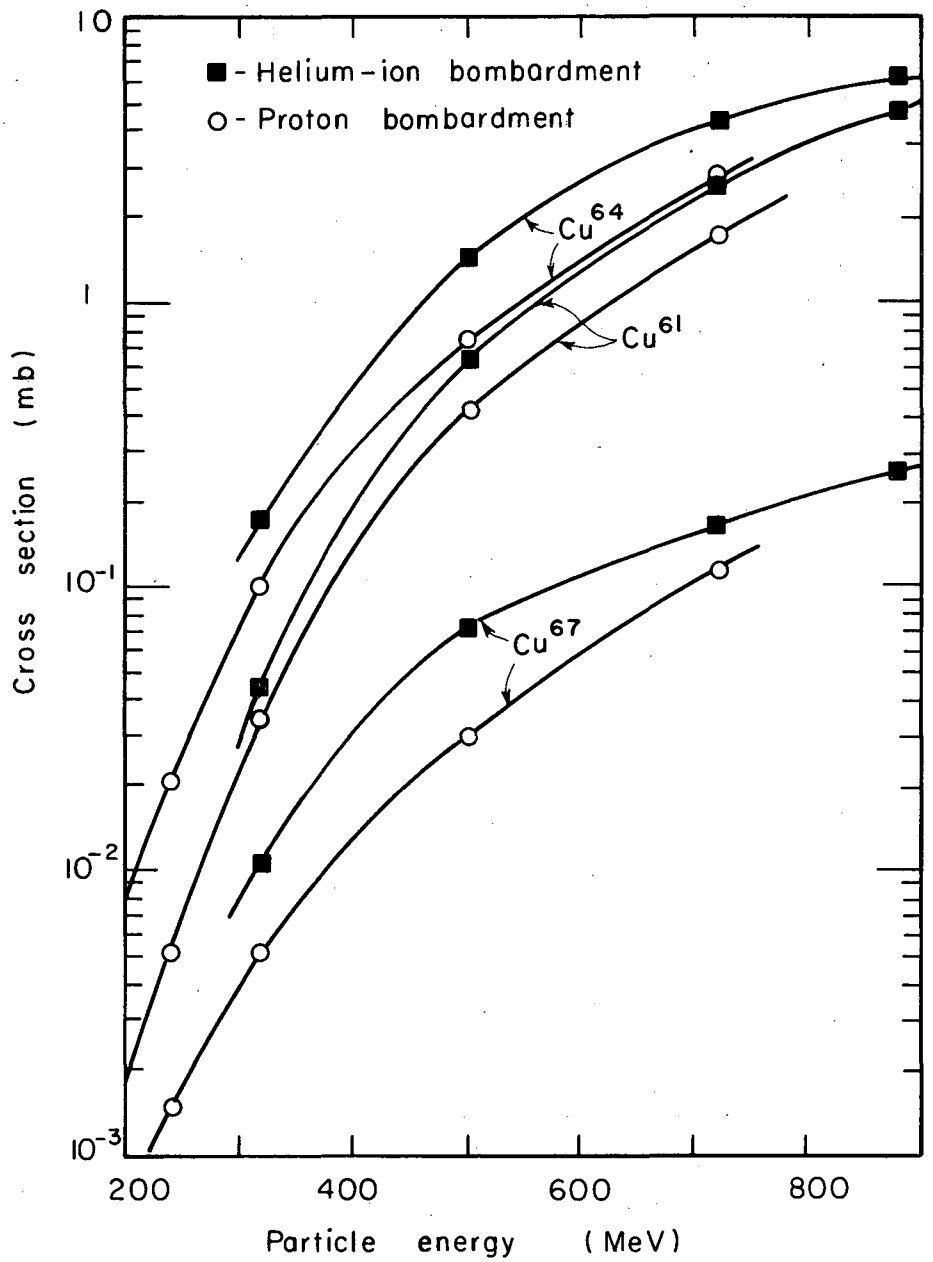

MUB-2766

Fig. 3

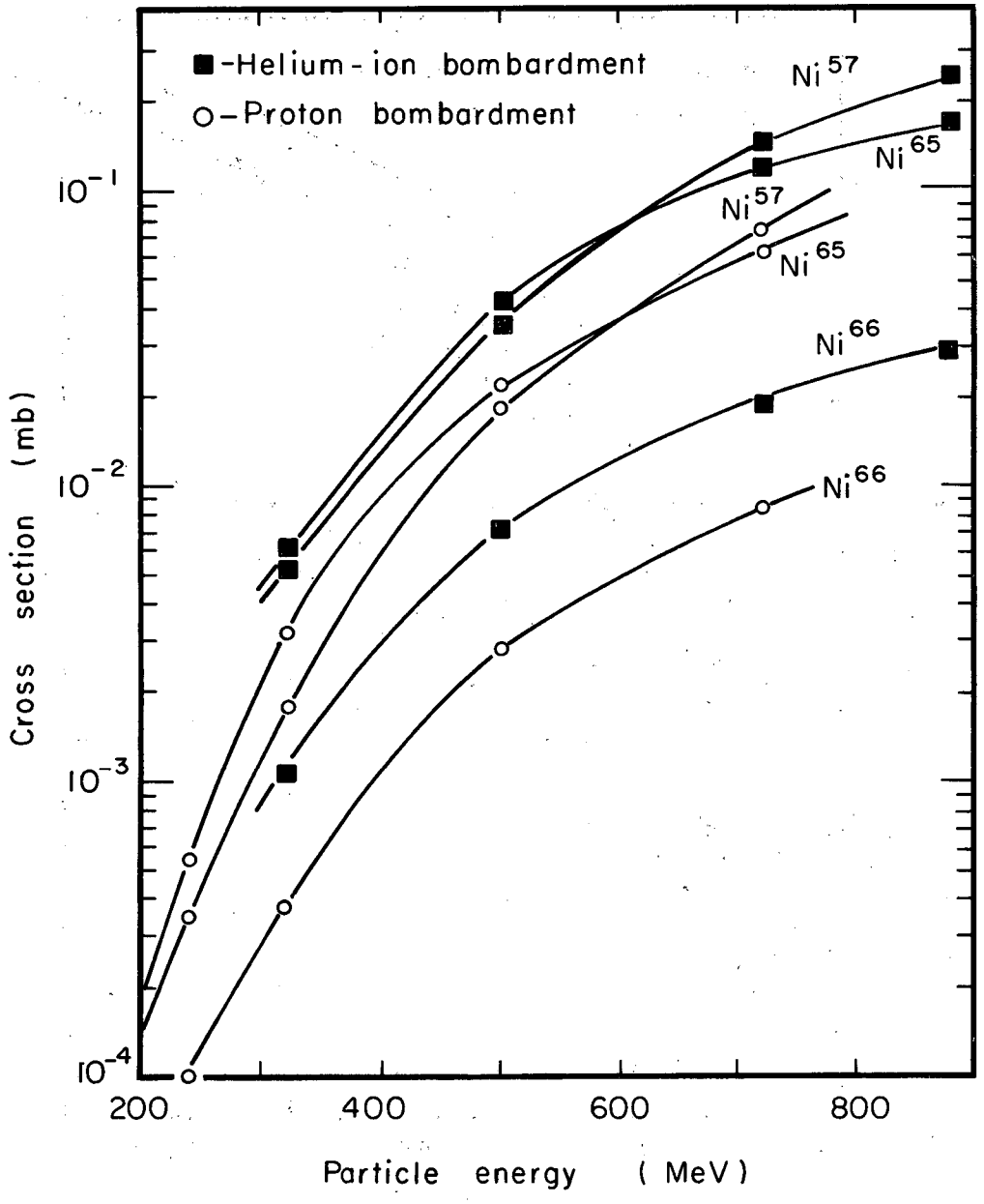

MUB-2767

Fig. 4

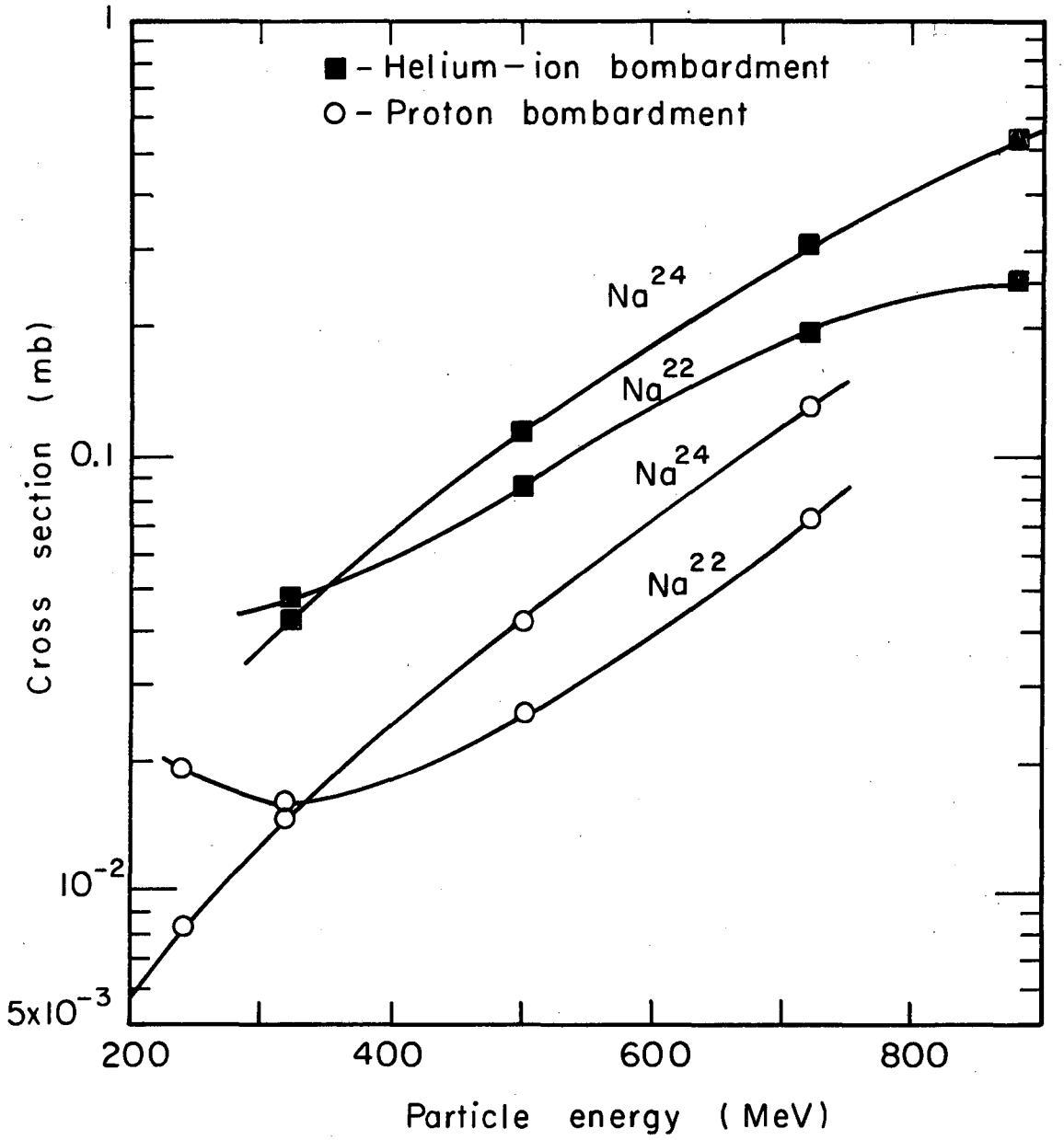

MUB-2768

Fig. 5

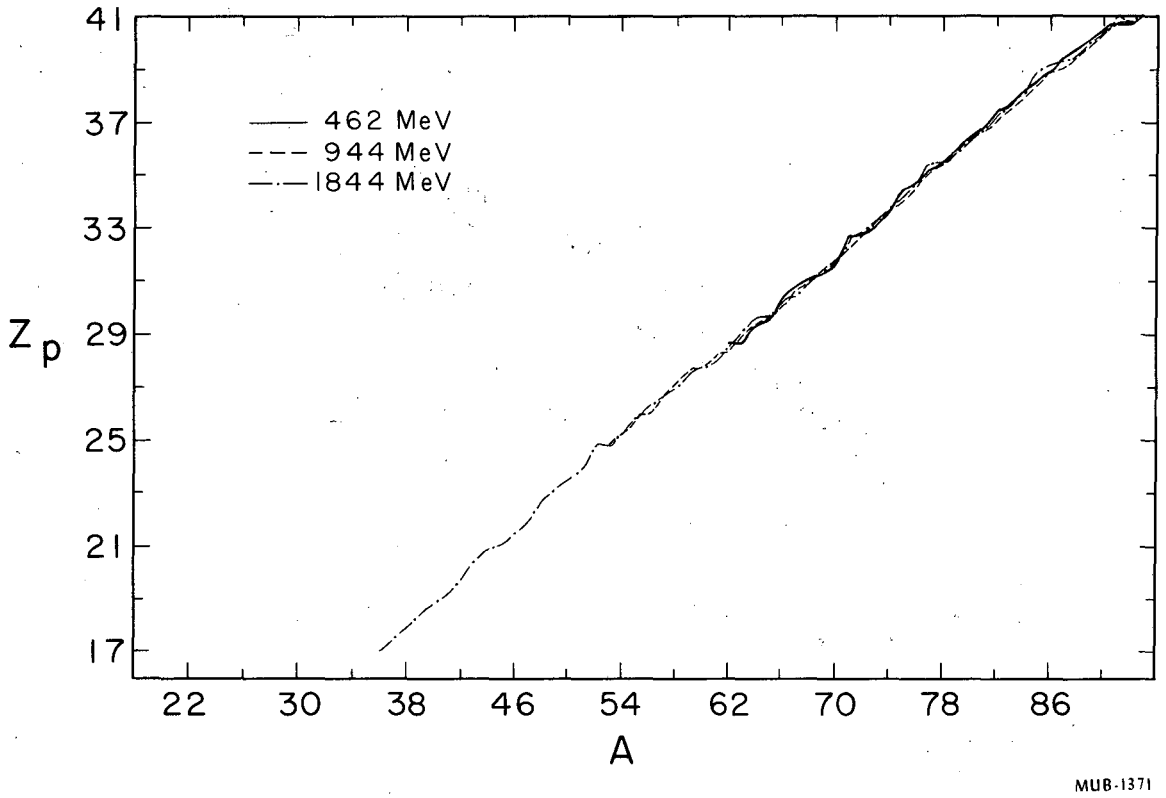
41
37
33
29
25
21
17
Z_p
462 MeV
944 MeV
1844 MeV
22
30
38
46
54
62
70
78
86
A
MUB-1371

Fig. 6

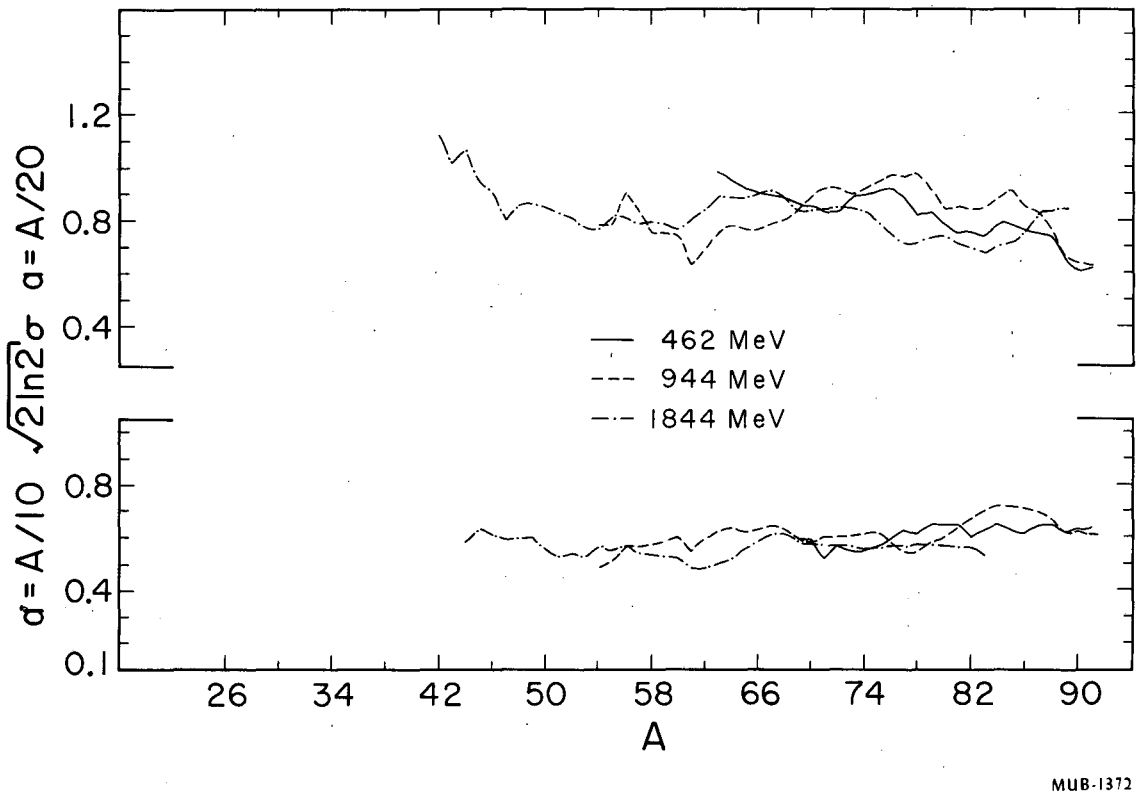
1.2
0.8
0.4
0.8
0.4
0.1
$\sqrt{2\ln 2}\,\sigma$ a = A/20
a = A/10
462 MeV
944 MeV
1844 MeV
26
34
42
50
58
66
74
82
90
A
MUB-1372

Fig. 7

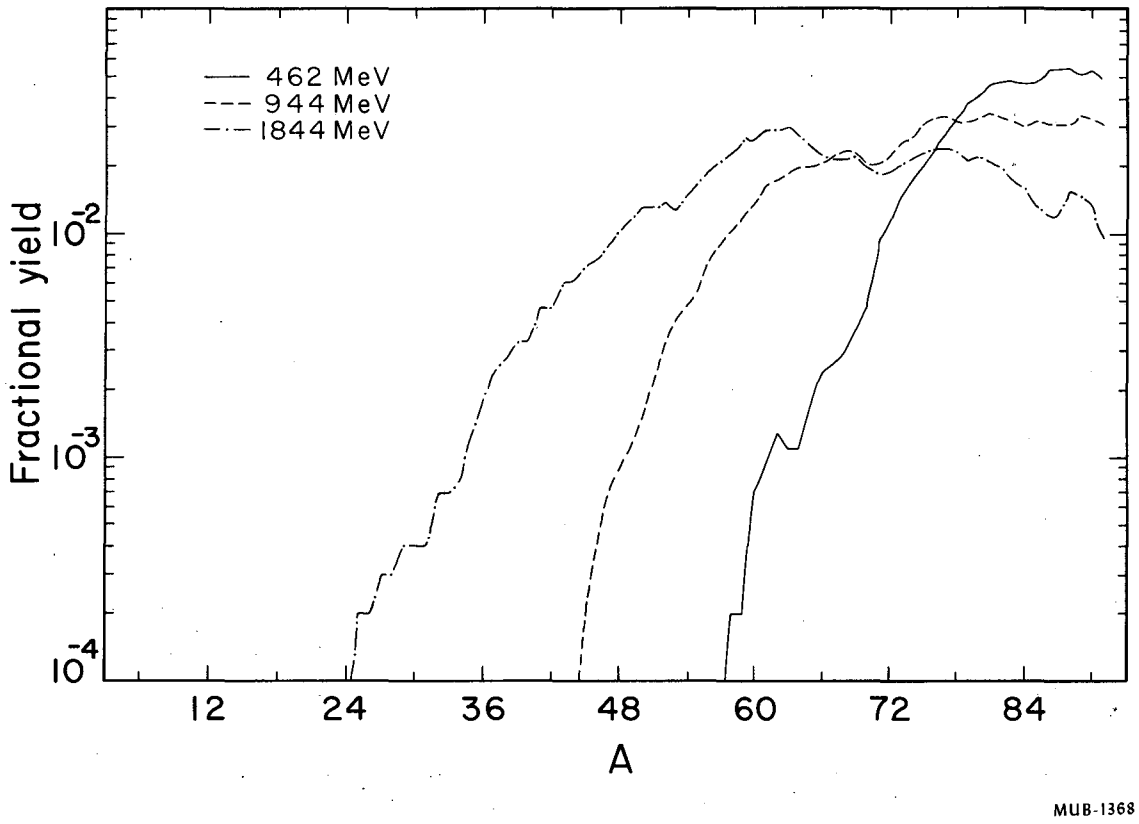
462 MeV
944 MeV
1844 MeV
Fractional yield
10^{-2}
10^{-3}
10^{-4}
12
24
36
48
60
72
84
A
MUB-1368

Fig. 8

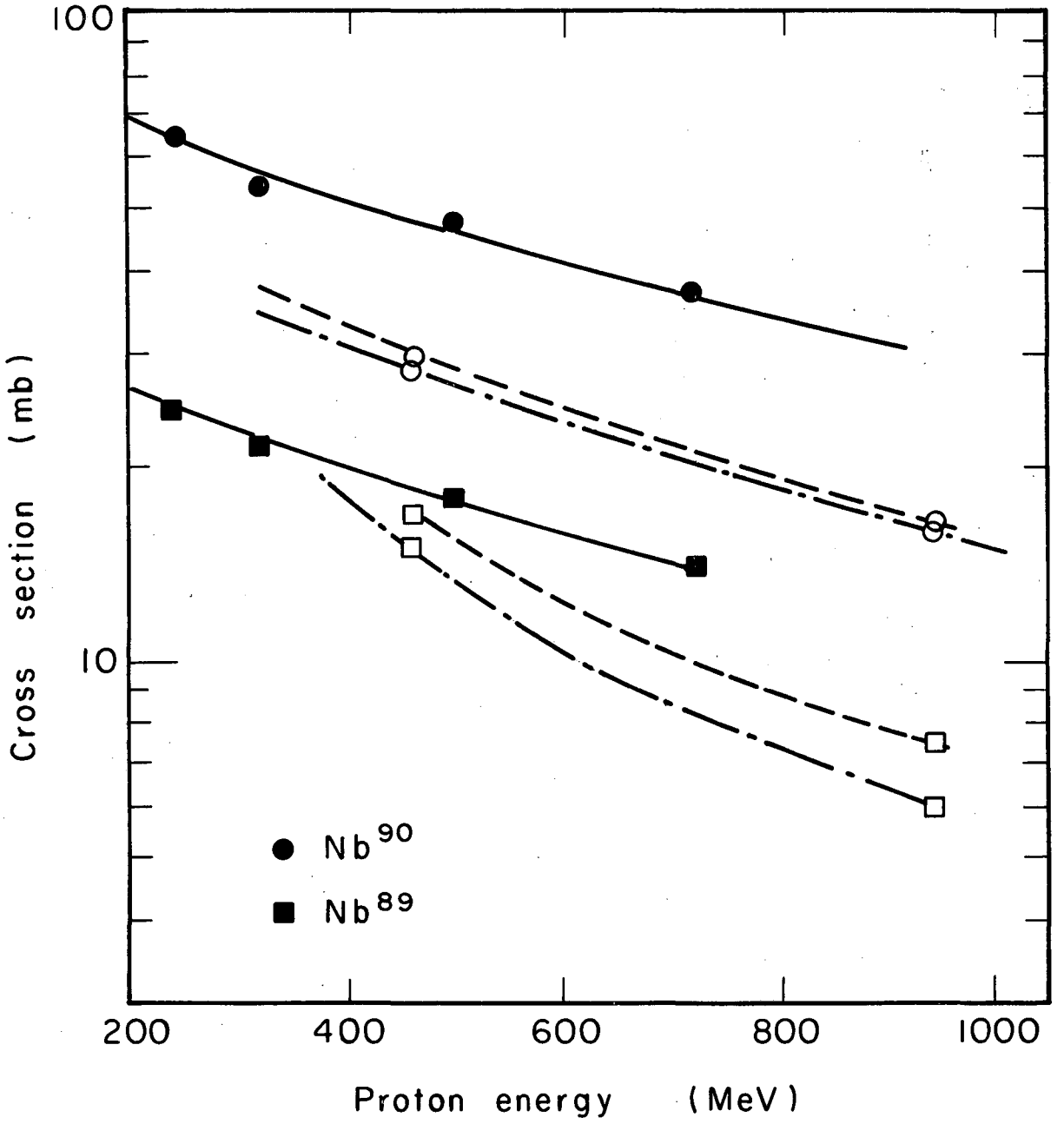

MUB-2784

Fig. 9

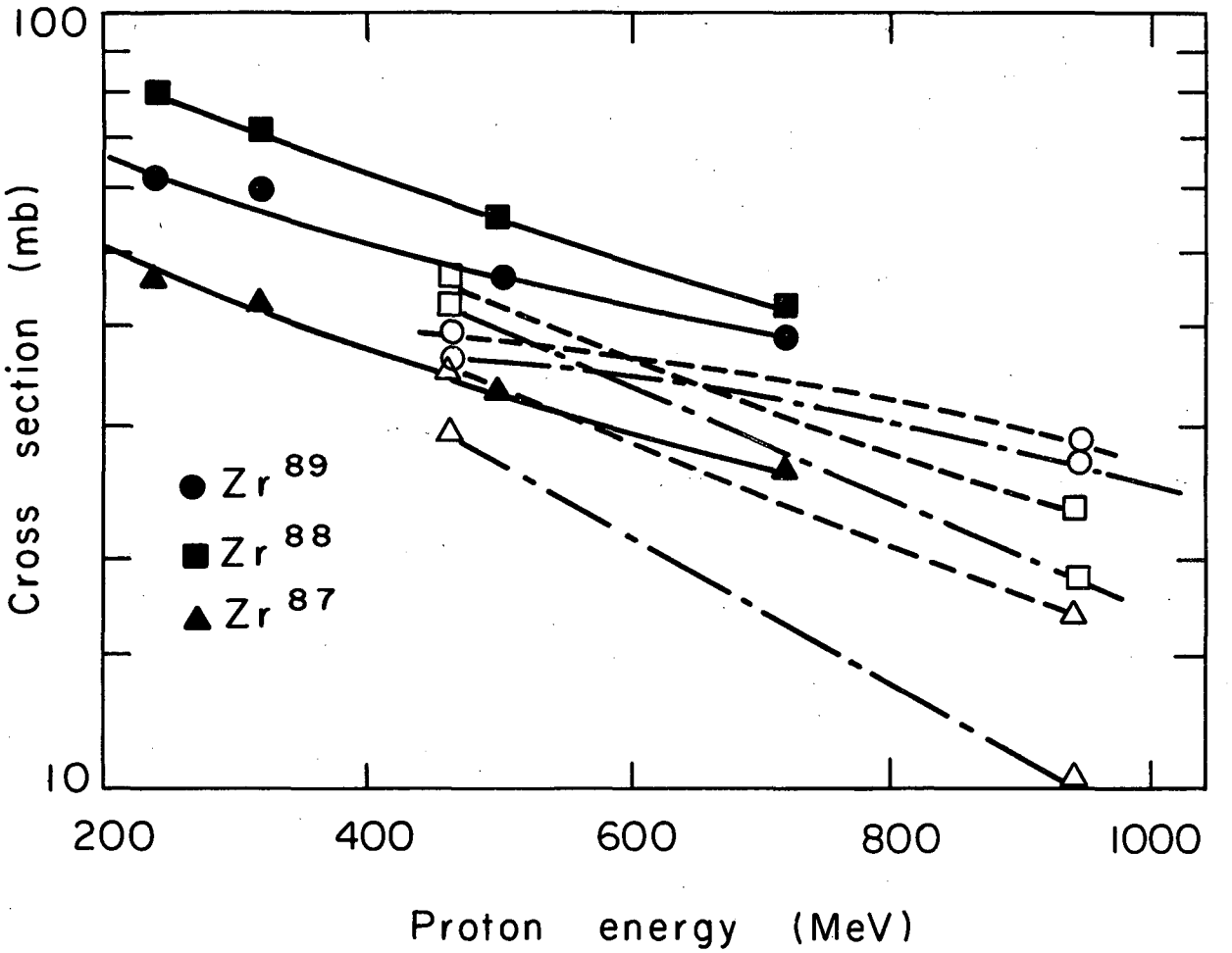

MUB-2785

Fig. 10

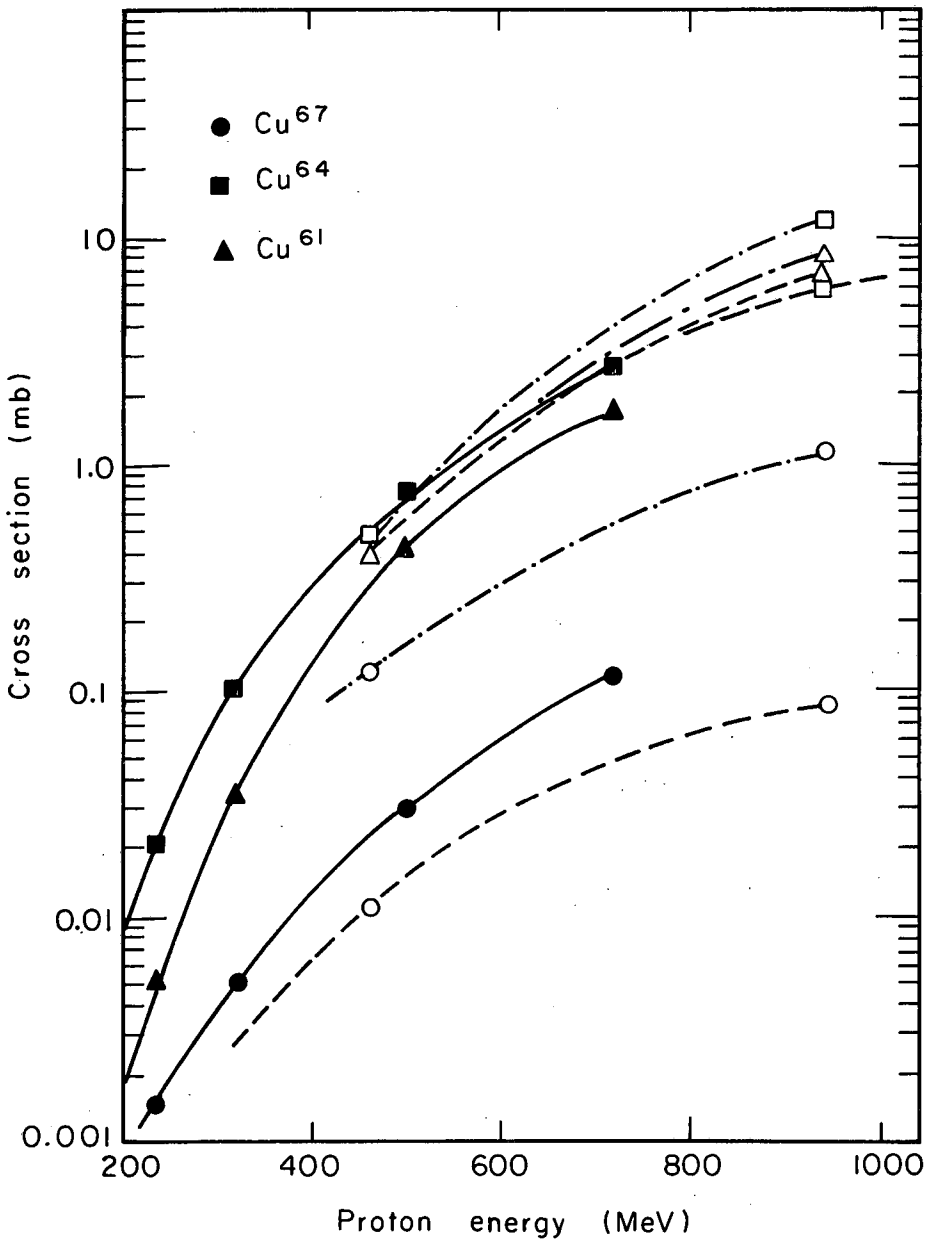

MUB-2786

Fig. 11

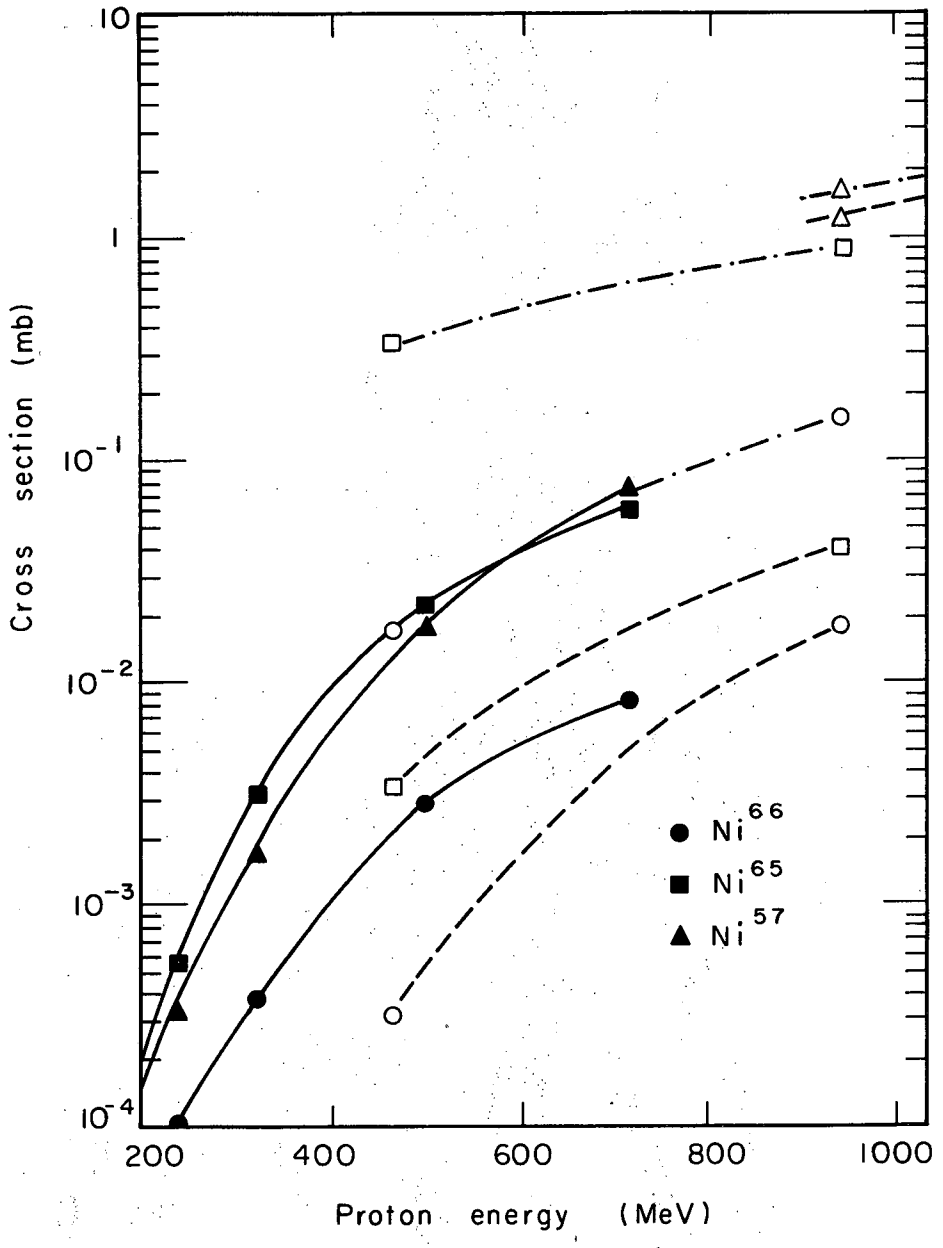

MUB-2787

Fig. 12

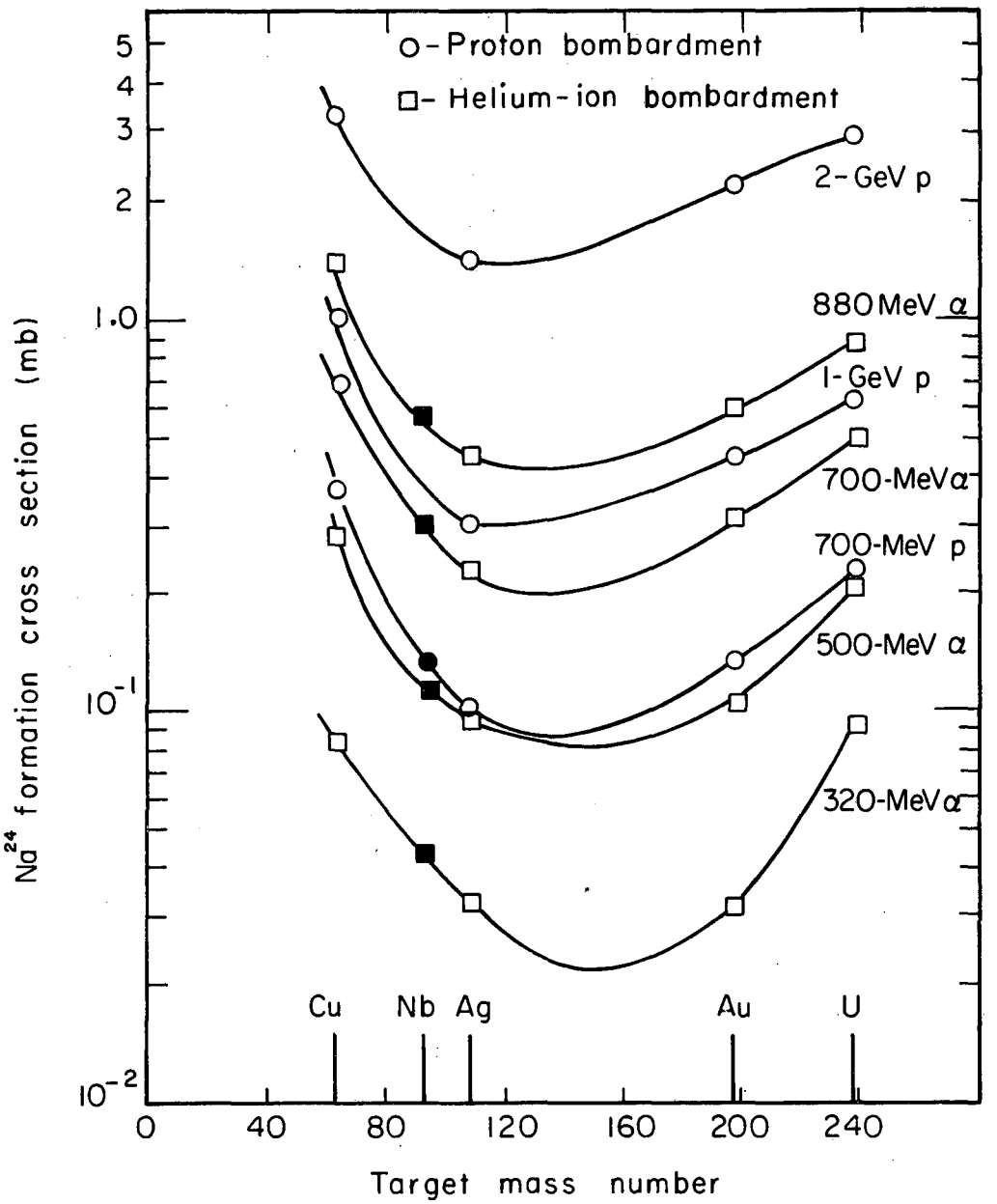

MUB-2769

Fig. 13

This report was prepared as an account of Government sponsored work. Neither the United States, nor the Commission, nor any person acting on behalf of the Commission:

A. Makes any warranty or representation, expressed or implied, with respect to the accuracy, completeness, or usefulness of the information contained in this report, or that the use of any information, apparatus, method, or process disclosed in this report may not infringe privately owned rights; or

B. Assumes any liabilities with respect to the use of, or for damages resulting from the use of any information, apparatus, method, or process disclosed in this report.

As used in the above, "person acting on behalf of the Commission" includes any employee or contractor of the Commission, or employee of such contractor, to the extent that such employee or contractor of the Commission, or employee of such contractor prepares, disseminates, or provides access to, any information pursuant to his employment or contract with the Commission, or his employment with such contractor.